ARCHER

Collaborative Project

Co-funded by the European Commission under the
Euratom Research and Training Programme on Nuclear Energy
within the Seventh Framework Programme

Grant Agreement Number: 269892
Start date: 01/02/2011Duration: 48 Months

www.archer-project.eu

Archer
Advanced Reactor
for Cogeneration of
Heat & Electricity-R&D

Deliverable D42.31: Review and data collection

Andreas Klenk, Magdalena Speicher (MPA Stuttgart)

ARCHER project – Contract Number: 269892
Advanced High-Temperature Reactors for Cogeneration of Heat and Electricity R&D
EC Scientific Officer: Dr. Panagiotis Manolatos

Document title	Review and data collection
Author(s)	Andreas Klenk (USTUTT-MPA), Magdalena Speicher (USTUTT-MPA)
Number of pages	55
Document type	Deliverable
Work Package	WP4.2
Document number	D42.31 – revision 0
Issued by	Materialprüfungsanstalt Universität Stuttgart (USTUTT-MPA)
Date of completion	15/01/2014
Dissemination level	Restricted to the partners of the ARCHER project

Summary

This document contains the literature review on the effect of microstructure, heat treatment, welding process and welding parameters on various types of cracks (solidification cracking, liquidation cracking and/or ductility dip cracking, relaxation cracking) in Alloy 800 H.

Approval

Rev.	Short description	First author	WP Leader	SP leader	Coordinator
0	First issue	Klenk, A (MPA)		Buckthorpe, D. 04/04/2014	S. Knol (NRG) 04/04/2014

Distribution list

Name	Organisation	Comments
P. Manolatos	EC DG RTD	
All technical participants	ARCHER	
Steering Committee members	ARCHER	

Table of contents

Abbreviations and Symbols

+A	Soft annealing
+AT	Solution annealing
+RA	Recrystallisation annealing
AR	As Received
ASTM	American Society for Testing and Materials
AWS	American Welding Society
bcc	body centred cubic
BTR	Brittle-Temprerature-Range
CPTT	Cast Pin Tear Test
Cr_{eq}	Chromium equivalent
DDC	Ductility Dip Crack
DRR	Ductility Recovery Rate
DTR	Ductility Temperature Range
DVS	German Association for welding and allied processes e. V. (Deutscher Verband für Schweißen und Verwandte Verfahren e.V.)
E-Hand	Manual metal arc welding
EN	European norm
fcc	face centred cubic
FCC_A1N1	Phase boundary 1 Nickel matrix
FCC_A1N2	Phase boundary 2 carbon nitride
IIW	International Institute of Welding
GMAW	Gas metal arc welding
MAG	Metal active gas welding
MIG	Metal inert gas welding
NDR	Temperature range of nil ductility
NDT	Nil ductility temperature
Ni_{eq}	Nickel equivalent
NST	Nil strength temperature
P	Plate
PAW	Plasma arc welding
PER	Perchlorethylene
PJW	Plasma jet welding
PM	Parent Material
PDC-Test	Programmed deformation crack test
PW	Plasma welding
RDR	Ductility recovery ratio
R&D	Research & Development
R_m	Tensile strength
SAW	Submerged-arc welding
SMAW	Shielded metal arc welding
SEW	Steel-Iron material sheet
Sim.	Simulation
SM	Sheet Metal
Spec.	Specimen
STF	Strain-To-Fracture
T_S	Absolute melting temperature
TEM	Transmission Elektron Microscopy
TIG	Tungsten inert gas welding
TIS	Temperature interval of brittleness
TTT	time temperature transformation

UNS	Unified Numbering System for Metals and Alloys
UV	ultraviolet radiation
VdTÜV	German technical inspection associations
W. -Nr.	Material number
ZDR	Temperature range of nil ductility
Z	Area reduction at fracture

Symbols

η	Efficiency
a	Acceleration
E	energy input per unit length
I	Welding current
L_r	Distance from the start of the seam until the occurrence of first solidification crack
Q	Heat input
$R_{m/t/T}$	Creep strength of the base material
$R_{m(w)/t/T}$	Weld creep strength
WSF	Welding strength factor
t	Time
T	Temperature
U	Arc voltage
v	Welding speed
v_{kr}	Deformation speed

Chemical Elements

Al	Aluminium
Al_2O_3	Aluminium oxide
Ar	Argon
B	Boron
C	Carbon
CO_2	Carbon dioxide
Co	Cobalt
Cr	Chromium
Cu	Copper
Fe	Iron
H_2	molecular Hydrogen
He	Helium
Mg	Magnesium
Mn	Manganese
Mo	Molybdenum
N	Nitrogen
N_2	molecular Nitrogen
Nb	Niobium
Ni	Nickel
NiS	Nickel sulphide
O	Oxygen
P	Phosphorus
Pb	Lead
S	Sulphur
Si	Silicon
Ti	Titanium
V	Vanadium
W	Tungsten
Zr	Zirconium

1. Introduction

The objective of the review was to investigate the influence of the parameters microstructure (1), welding processes (2), stress conditions (4) and heat treatment conditions (5) on crack phenomena in Alloy 800 H. The review is intended to characterise the influence of these parameters on crack sensitivity and is prepared with regard to possibilities of crack prevention during and after welding.

2. Alloy 800 - Basic information

Alloy 800 H is a nickel-iron-chromium-(Ni-Fe-Cr) alloy and belongs to the solid solution hardening nickel alloys. The internationally most common types of Alloy 800 H and their variants are shown in **Table 2-1**. Other international standard names of the alloy are attached in **Appendix A.**

Material	EN Material short name	Alloy	UNS
1.4876	X5NiCrAlTi 31-20	Alloy 800	N 08800
1.4958	X8NiCrAlTI 32-21	Alloy 800H	N 08810
1.4959	X8NiCrAlTi 32-21	Alloy 800HT	N 08811

Table 2-1: International designation of Alloy 800 H [1]

In addition, registered trade names are used as a synonym for the nickel base alloy Alloy 800 H, the most common names are:

- Nicrofer® 3220H (ThyssenKrupp AG)
- Incoloy® 800H (Special Metals Corporation)
- Sanicro® 31H (Sandvik AB)

2.1 Microstructure

In addition to the main elements nickel, chromium, and iron Alloy 800 H contains controlled amounts of carbon, aluminium, titanium, silicon and manganese, as well as a controlled total content of Al + Ti [2].

The chemical composition in weight percent of the nickel alloys of type 800 is specified in **Table 2-2**.

Alloy		Ni	Cr	Fe	C	Mn	Si	Cu	Al	Ti	Al+Ti	P	S
800	min.	30,0	19,0	Bal.	-	-	-	-	0,15	0,15	-	-	-
	max.	34,0	23,0		0,12	2,0	1,0	0,75	0,60	0,60	0,7	0,030	0,020
800H	min.	30,0	19,0	Bal.	0,06	0,5	0,2	-	0,20	0,20	-	-	-
	max.	32,0	21,0		0,08	1,0	0,6	0,50	0,40	0,50	0,7	0,015	0,010
800HT	min.	30,0	19,0	Bal.	0,06	0,5	0,2	-	0,30	0,30	0,85	-	-
	max.	32,0	22,0		0,10	1,0	0,6	0,50	0,60	0,60	1,20	0,015	0,010

Table 2-2: Chemical composition of the Alloy-800 series, wt -% [2]

Depending on the composition of the Ni-Fe-Cr alloys two primary phases of solidification are possible, austenitic (γ), or delta-ferritic (δ). Usually alloys with high chromium and low nickel content show a primary δ-ferritic solidification. However alloys in which the Ni content predominates, solidify primarily to austenite [3]. In **Figure 2-1** the ternary Ni-Fe-Cr system is shown for the evaluation of solidification. Here, the Fe-Ni-range represents the γ-solid solution, and thus the austenite, whereas the Cr-Fe-range represents the δ-ferrite.

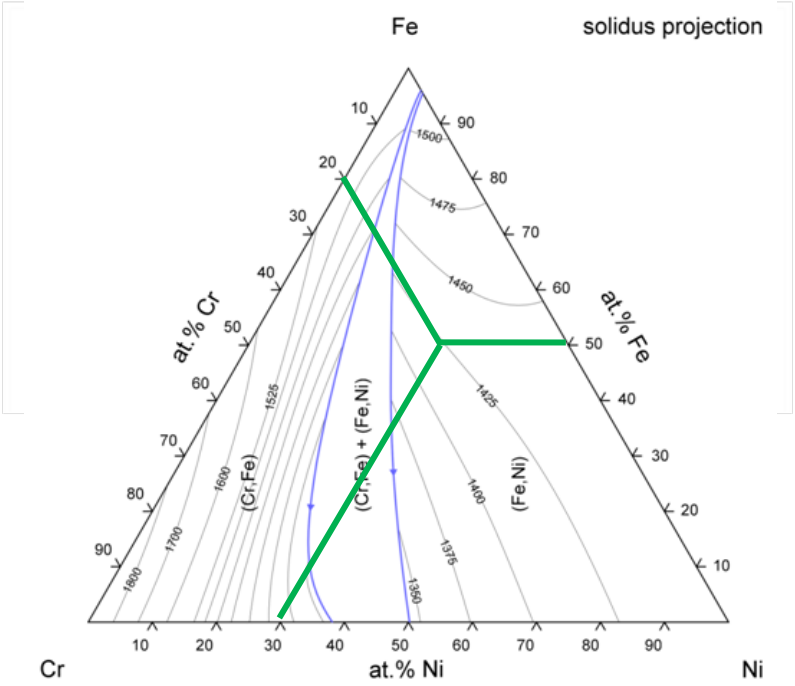

Figure 2-1: Phase diagram of the Ni-Fe-Cr system with marked Alloy 800 H [4]

According to Figure 2-1 the composition of nickel alloy Alloy 800H leads to an austenitic microstructure of the material with a melting or solidification temperature of about 1400°C. The alloy is a solid solution-forming and -strengthening Ni-Fe-Cr alloy, which has a face centred cubic lattice structure as the result of the austenitic microstructure [2], [5].

Using appropriate alloying elements, the solid solution formation of Ni-Fe-Cr alloy can be targeted specifically, allowing increased heat resistance and scaling resistance [6].

Alloy 800H is usually delivered in the solution annealed condition [2]. This is because any existing carbide precipitates, delta-ferrite and sigma phase, as well as production-related strain hardening can be excluded. A solution-annealed delivery condition is usual for alloys with high nickel content [7].

In **Figure 2-2** a microstructure of Alloy 800 H is shown. The relatively large grains typical of an austenitic structure are seen. Furthermore, twin grains are present resulting from the manufacturing related solution annealing.

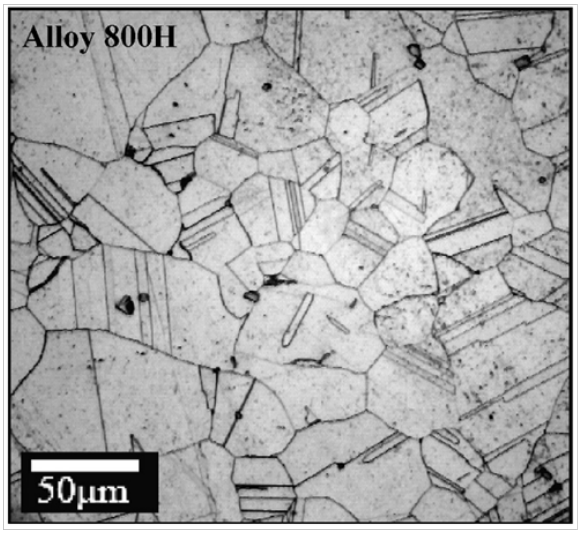

Figure 2-2: Microstructure of Alloy 800H [7]

The austenitic matrix also contains titanium nitride, plus titanium and chromium rich carbides [5]. In addition to the resulting increased creep resistance above 600°C, the controlled Al + Ti total content of max 0.7% serves to avoid a loss of toughness, and makes possible a long term use at temperatures between 500° and 700°C. The high nickel and chromium content lead to an excellent oxidation resistance and a high resistance to hydrogen [5].

Furthermore, the alloy has a good resistance to reduction, nitrating and oxidising atmospheres as well as atmospheres which alternate between reducing and oxidising conditions [5].

2.2 Grain structure

The nickel base alloys Alloy 800, 800 H and 800HT have similar chemical compositions, as shown above in **Table 2-2**. However Alloy 800H and 800HT have, in contrast to Alloy 800, significantly higher creep strength above 600°C. This property is due to a larger grain size [8]. The solution annealed alloy Alloy 800 H has a grain size between 70 to 180 µm [2], [5]. For use at temperatures below 600°C, a soft annealed alloy is recommended which has a grain size below 64 µm.

With the help of the grain boundary engineering (GBE), it is possible to improve the properties of various materials or adapt them specifically to the material requirements. Optimization of grain boundary distribution can be achieved by thermomechanical processing. The thermomechanical processing of Alloy 800H performed in [9] was carried out in stages of cold forming, high temperature annealing with water quenching and thermomechanical processing to reduce the thickness by 6%, followed by annealing at 1050°C for 90 minutes.

The results in [9] show that the GBE treatments reduce heavily oxide spalling in Alloy 800 H. At the same time the room temperature strength of Alloy 800 H could be improved by more than 10%.

Further investigation [10] showed that using GBE extension of Σ3n grain boundaries by up to 70% is possible, whereby the resistance of grain boundary diffusion in Alloy 800 H can be increased, see **Figure 2-3**. The GBE treatment was carried out in this case by 4 cycles of cold rolling and annealing.

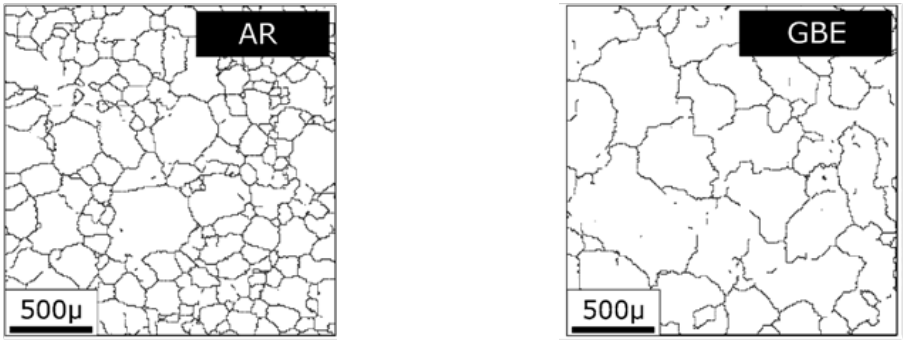

(a) (b)

Figure 2-3: Grain boundaries in (a) AR - As Received and (b) of a GBE-treated sample [10]

The experiments carried out in [11] are concerned with nucleation mechanisms during dynamic recrystallisation (DRX) and the impact on the flow behaviour of Alloy 800H. The results of tensile tests carried out here are shown in the stress-strain diagrams, **Figure 2-4**.

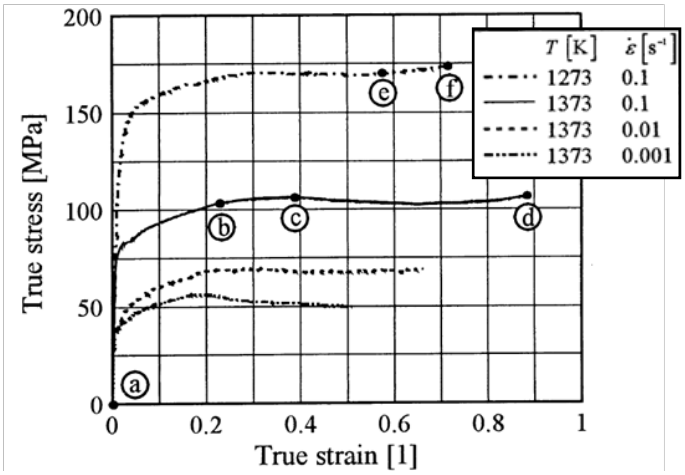

Figure 2-4: Yield curve of Alloy 800H under different loading [11]

It can be seen that the maximum stress decreases significantly with decreasing strain rate έ. The optically evaluated development of the grain structure during dynamic recrystallisation at temperatures of 1373 K (~ 1100°C) and a strain rate έ = 1 * 10¯1s¯1 is shown in **Figure 2-5**.

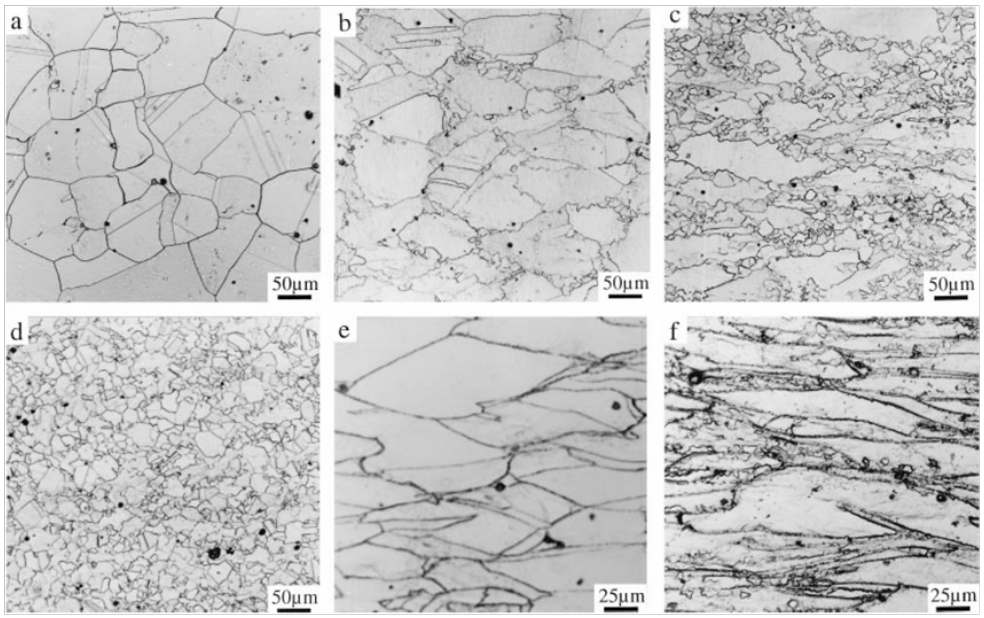

Figure 2-5: Development of the microstructure at T = 1373K, έ = $1_{*}10^{-1}s^{-1}$: a) ε =0, b) ε =0.23, c) ε = 0.39, d) ε = 0.89; T = 1273K, έ = $1_{*}10^{-1}s^{-1}$: e) ε = 0.58, f) ε = 0.73 [11]

The initial microstructure of Alloy 800H shows uniform grains with an average size of 70 microns and typical annealing twins (**Figure 2-5** a). Even at low strain (Figure 2-5 b), the grain boundaries are indistinct and show bulges. In addition, some new small recrystallised grains can be seen at the grain boundaries particularly at the triple points, which increase with increasing strain (Figure 2-5 c). At higher strains, the initial grain structure is replaced by small grains aligned equiaxially with grain size of 10 µm (Figure 2-5d), which remain stable upon further deformation [11].

Wang [12] investigated the nucleation mechanisms of dynamic recrystallisation based on alloy Alloy 800H and came to the same conclusions that a dynamic recrystallisation in areas of grain boundaries begins regardless of bulges.

Furthermore, Wang [13] determined that the twin formation during nucleation and growth of dynamically re-crystallised grains in Alloy 800 H is important. Twinning is an active nucleation mechanism at the DRX which promotes recrystallisation.

Tan [9] showed for grain boundary precipitates based on statistical analysis that that the morphology and their distribution is dependent on grain boundary type. Basically, grain boundaries are divided into three different types, as shown schematically in **Figure 2-6** [3].

- Solidification Subgrain Boundaries
- Solidification Grain Boundaries
- Migrated Grain Boundaries

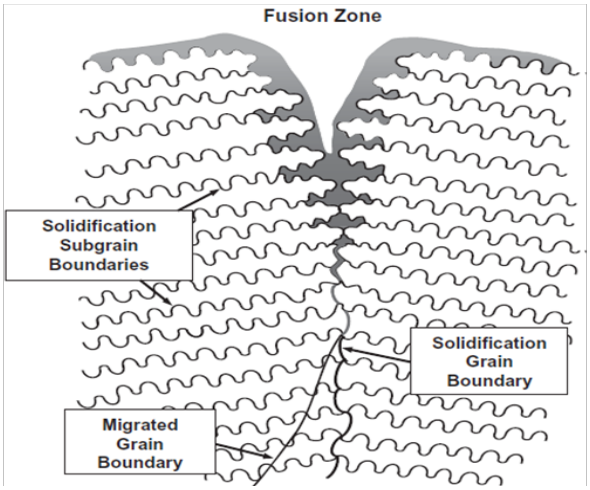

Figure 2-6: Schematic diagram of grain boundaries [3]

2.3 Precipitation structure

Table 2-3 shows the effect of various alloying elements on the phase stability in nickel alloys.

Effect	Element
Solid solution strengthening effect	Co, Cr, Fe, Mo, W, Ta
γ'-Ni_3(Al, Ti) former	Al, Ti
Solid solution strengthening effect of γ'	Cr, Mo, Ti, Si, Nb
γ''-Ni_3Nb former	Nb
Carbide former	
▪ MC and M(C,N)	W, Ta, Ti, Mo, Nb
▪ M_7C_3	Cr
▪ $M_{23}C_6$	Cr, Mo, W
▪ M_6C	Mo, W
TCP Phases (σ, P, μ, Laves)	Ti, V, Zr, Nb, Ta, Al, Si
Formation of surface oxides (Cr_2O_3 / Al_2O_3)	Cr, Al

Table 2-3: Influence of alloying elements on the phase stability in nickel base alloys [3]

In addition to the solid solution strengthening Alloy 800H receives additional hardening due to the precipitation of titanium carbon nitride (Ti (C, N)) and chromium-rich mixed carbide of the $M_{23}C_6$ type ($(FeCr)_{23}C_6$) [14].

The precipitation of titanium carbon nitride, a solid solution of titanium carbide and titanium nitride is characterized by the high hardness of titanium carbides and the chemical resistance of the titanium nitride. In addition, titanium carbon nitrides have a high thermal conductivity [15].

In general, MC carbides form at the end of solidification by eutectic reactions with the γ-matrix. The structure of these carbides is face centred cubic. The M (CN) carbon nitrides are very similar to the MC carbides, except that a high proportion of carbon (C), is replaced by nitrogen (N) [3]. Because of the strong affinity to C, N, and a number of metal elements (in particular Ti and Nb), the eutectic reaction and the associated types of carbides and carbon nitrides are stimulated to precipitate from the liquid during solidification. This results in an increased occurrence of the MC-carbides in the areas along the interdendritic and solidifying grain boundaries [3].

Due to heat treatment and / or high-temperature use, there is the possibility that the MC carbides are replaced by $M_{23}C_6$- and M_6C carbides [3]. The formation of M_6C carbides takes place usually if a Mo and / or W content is higher than 6-8 atomic percent, which is why they are unimportant with regard to the nickel alloy Alloy 800H without the influence of molybdenum or tungsten-containing weld fillers, see Table 2-2 [3].

The chromium-rich $M_{23}C_6$ carbides are formed usually in areas with a cubic crystal structure and temperature of 760 to 980 °C. Predominantly these carbides form at the grain boundaries, resulting in an increase of creep rupture strength by impeding grain boundary sliding [3].

In solution-annealed stainless steels and nickel base alloys the nucleation sites for carbides are mainly the grain boundaries. In addition the total grain boundary area increases with the decrease of the grain size. Therefore, the probability of the formation of a continuous network of grain boundary carbides decreases the smaller the grain size is. Thus a positive effect can be assumed by smaller grain sizes. It follows that a subsequent annealing should be carried out for materials which are exposed to solutions causing intercrystalline attack during processing by cold forming, whereby a small-grained microstructure can be guaranteed [16].

Aigner [17] examined precipitations on aged samples. The ageing treatment was carried out at temperatures of 800°, 900° and 1000°C and the respective ageing times of 6, 25, 100, 400 and 900 h. In addition, annealing was carried out in an argon containing atmosphere to prevent surface reactions. After 6 hours of ageing at 800°C, an increase of the 0.2% yield strength by about 25% compared to the initial state could be observed due to carbide precipitation. TEM studies performed in [17] also revealed that the carbide formation occurs particularly in heavily disturbed areas along the grain boundaries, where dislocations accumulate in slip planes. The carbide precipitates identified as $M_{23}C_6$ occur with a fine structure after exposure for 6 hours, whereas a significant coarsening of the precipitates can be noted after 25 h ageing. Due to these precipitates the 0.2% yield strength and tensile strength increases initially after 100 hours at temperature of 900°C. With continuation of ageing and the related coarsening of precipitates a steady decrease of the strength values is recorded. At ageing temperatures of 1000 °C, the yield strength steadily falls [17].

Taylor [18] examined the carburisation of Alloy 800H at a temperature of 800 °C. The carburisation was carried out at 1000°C in a gas mixture of H_2/CH_6 under an appropriate pressure for a carbon activity of 0.8. The carburised samples had a structure consisting of an outer layer of M_7C_3 and an inner zone of $M_{23}C_6$.

However, the exclusion of oxygen in the atmosphere through the oxide-forming elements Cr, Al and Si, which are nitride formers at the same time, leads to the conversion of the oxides formed previously into nitrides. This reduces both the notched impact strength and the oxidation resistance of the material [19].

In nitrogen, nitrogen-hydrogen or ammonia-containing atmospheres Alloy 800H tends to react with the nitrogen. Depending on the temperature, the gas and the alloy composition a nitridation or nitriding process occurs due to the ingress of nitrogen into the material. This results in the formation of nitride surface layers and / or nitrides inside the material. The carbides of the type $M_{23}C_6$ occurring here are converted to nitrides due to the nitridation process. These processes lead to hardening of the material, which reduces the notched impact strength [19]. At the same time strains occur due to the nitride formation, due to its lower density compared to the base matrix [19].

Dehmolai [20] analysed the microstructure of Alloy 800 before and after 15 years in operation. The material was used in reformer tubes under operating conditions of hydrogen-containing atmosphere and temperatures of 815 °C. Objectives were the formation and growth of secondary precipitates, phase transformation of titanium carbide to $Cr_{23}C_6$ and $Ni_{16}Ti_6Si_7$ (G-phase) and the decomposition of the primary carbides.
Dehmolai demonstrated transformation of some solid solutions into carbides during operation. The formation of precipitates identified as chromium carbide ($Cr_{23}C_6$) occurs in a temperature range 600 to 850 °C. In this temperature range, in contrast to the titanium atoms, a faster diffusion of chromium atoms in the austenite phase and in the grain boundaries is possible. Simultaneously the carbon dissolved in the austenitic matrix moves in the direction of the grain boundaries, whereby the chromium diffuses along and through the grain boundaries and reacts with carbon to $M_{23}C_6$ [20].

Due to the operating conditions the elements chromium, nickel and silicon present in the austenitic matrix diffuse to titanium carbide (TiC), where the carbon of the titanium carbide forms precipitations of Cr carbide or a mixed (Ti, Cr) carbide.

Because of the instability of titanium carbide at temperatures of ca 815°C a G-phase ($Ni_{16}Ti_6Si_7$) can also be formed during diffusion of nickel and silicon using the titanium of the titanium carbides, see **Figure 2-7 a** [20].

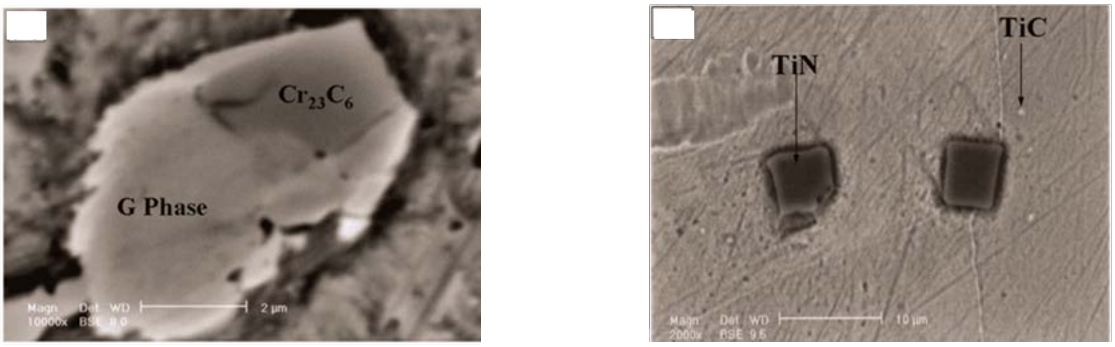

Figure 2-7: (a) REM image of G-Phase and $Cr_{23}C_6$ precipitate ; (b) REM-image of titanium nitrides and –carbides [20]

These changes increase the material embrittlement and cause poor weldability. In addition, the cubic precipitates were identified as titanium nitrides by EDS analysis, see **Figure 2-7 b**. The reason for the presence of these precipitates is the high operating temperature of 815°C initially described for the alloy and the increasing stability of the titanium nitrides approaching the melting temperature [20].

Moreover, according to [3], [2] a intermetallic secondary γ'-phase, can be formed by a specific heat treatment or a longer ageing of the Alloy 800 H below 700°C. The Ni-Al and Ni-Ti systems are the basis for the γ-γ'-precipitation hardened microstructures. The maximum solubility of each of Al and Ti in nickel is about 11 wt -%, at which the solubility decreases with increasing temperature and promotes precipitation strengthening reactions [3]. As a result, most alloys have a combined Al + TI content below 10 wt. %.

This results in the formation of intermetallic precipitates of the type Ni_3Al or Ni_3Ti [3]. In **Figure 2-8**, the crystal structure of the γ'-phase (Ni_3 (Ti, Al)) is shown schematically. The face centred cubic γ'-phase is present here in an ordered $L1_2$ phase, whereby there is a good crystallographic match with the face centred cubic nickel matrix [3].

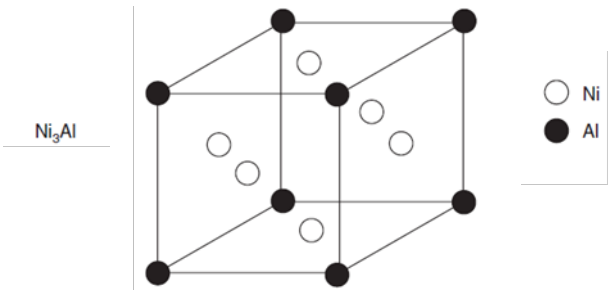

Figure 2-8: Crystal structure of the face centred cubic γ'-Phase [3]

Due to the γ'-phase and the associated precipitation hardening, the tensile strength and yield strength, based on standard Alloy 400 (material no. 2.4360; R_m = 450 MPa, $R_{p\ 0.2}$ = 180 MPa) [21] are nearly doubled [3]. Also the precipitation of the γ'-phase results in a loss in ductility of the alloy, which is compensated by maintaining a controlled content of Al + Ti [2].

In addition, topologically close packed phases (TCP) may occur during solidification. Further, the formation of these brittle phases can take place under elevated temperatures and sufficient time [3]. In general, these phases should be avoided due to the high hardness, brittleness and strength. The Sigma phase is not stable at temperatures above 1000 °C. An corresponding long ageing of the alloy at low temperatures allows the nucleation and growth of this phase [3]. The Sigma phase is stabilised with increasing Fe and Cr content and decreasing temperature. This stabilisation occurs due to the decrease of Fe - Cr-solubility in nickel with decreasing temperature.

A search in regard of Time-Temperature-Transformations (TTT) diagrams revealed that Baker [22], [23] presented without publication two TTT diagrams at a conference in 1964. These diagrams referred to the $Cr_{23}C_6$-carbide precipitation of a 0.033% C21Cr-33Ni alloy and a 0.07% C 21Cr-33Ni alloy.

Furthermore, according to [24] and [25] the precipitation of carbides starts from as early as 100 hours (the basis of the TTT-diagram by Lippold [26] for Alloy 800) in a temperature range of 540°C. Whereas materials operated below 480°C for several years do not exhibit any carbide precipitates.

Orr [27] published a TTT-diagram for Alloy 800 in 1978, see **Figure 2-9**. For the preparation of the diagram extensive investigations were carried out as reported.

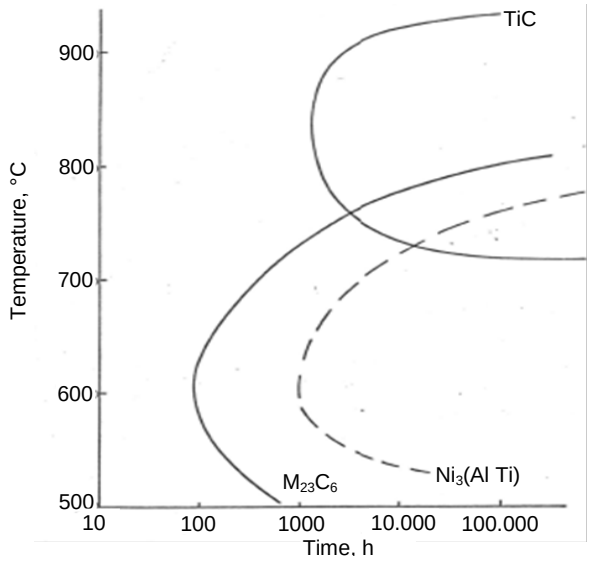

Figure 2-9: Time-Temperature-Transformation diagram of Alloy 800 [27]

In 1982 Jones [28] wrote that at that time no extensive systematic studies had been conducted, with which a time-temperature-precipitation diagram for Alloy 800 could be created. Thus an approximate diagram was created based on current information from the literature, see **Figure 2-10**.

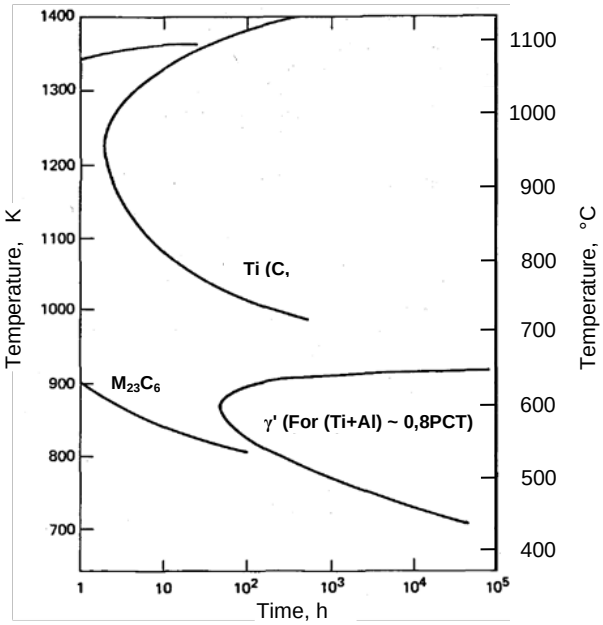

Figure 2-10: Approximate Time-Temperature-Transformation diagram of Alloy 800 [28]

A comparison with Figure 2-9 shows major differences. According to the diagram Figure 2-10, the formation of the $M_{23}C_6$ carbide occurs immediately at a temperature above ca 800 K (~ 530 °C). Nicolin [29] also found in his experiments a precipitation of $M_{23}C_6$ carbide after 8 h and at a temperature of 800 °C. The formation of the γ'-phase begins according to the graph from a duration of about 60 hours in a temperature range of about 870 K (~ 600 °C) with subsequent decreasing temperature. These data are consistent with the aforementioned statements regarding the formation of the γ'-phase at temperatures below 600 °C. Furthermore, a precipitation of Ti (C, N) is expected from temperatures above about 1000 K (~ 730 °C).

In addition, a report of the API committee (American Petroleum Institute Committee) was published in 2012 [30], in which a TTT-diagram for Alloy 800H was listed, see **Figure 2-11**. The precipitates depicted there were analysed using a TEM examination at 50,000-fold magnification. The focus of the report was on embrittling phases, thus the formation of G and σ-phase as well as the formation of Florenskyite (FeTiP) is shown in addition to those $M_{23}C_6$ carbides listed in Figure 2-9 and Figure 2-10.

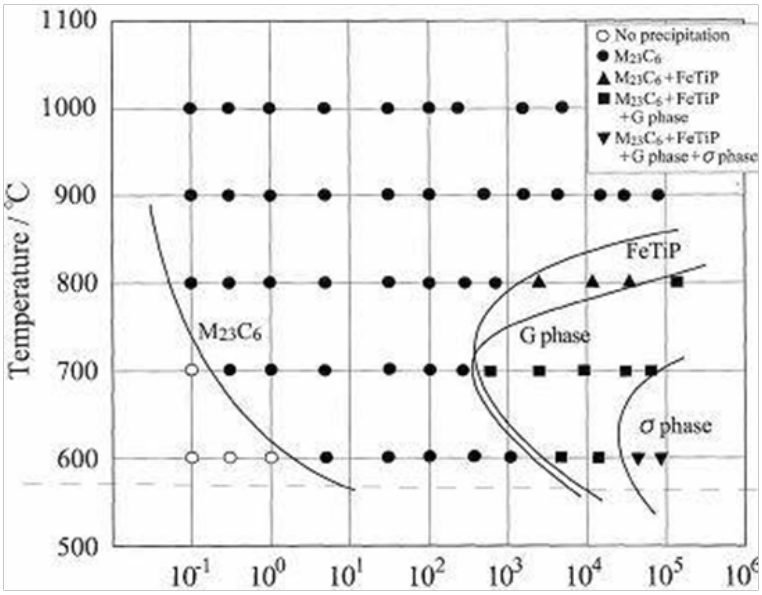

Figure 2-11: TTT diagram of Alloy 800H [30]

On the basis of systematic investigations using thermodynamic and diffusion computer programs (Thermo-Calc and Dictra[1]), Mizia [31] showed the possible precipitations of Alloy 800H. The objective of the research was understanding of the phase composition of Alloy 800H as a function of temperature and concentration of the various components. **Figure 2-12** represents the phase composition of Alloy 800H as a function of temperature.

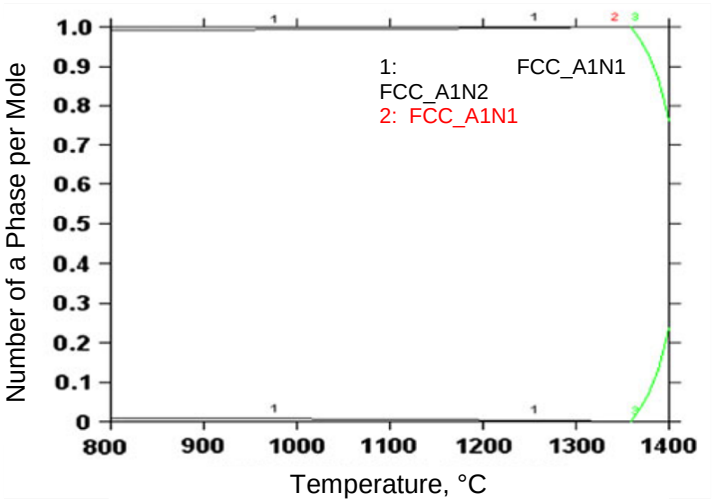

Figure 2-12: Phase composition of Alloy 800H as function of temperature [31]

It shows that in the temperature range 800 - 1320 ° C, the predominantly austenitic matrix contains a low fraction of titanium and niobium carbon nitrides, which begin to dissolve only above 1320 ° C. The volume fraction of titanium and niobium carbon nitrides is steadily below 0.5% in this temperature range.

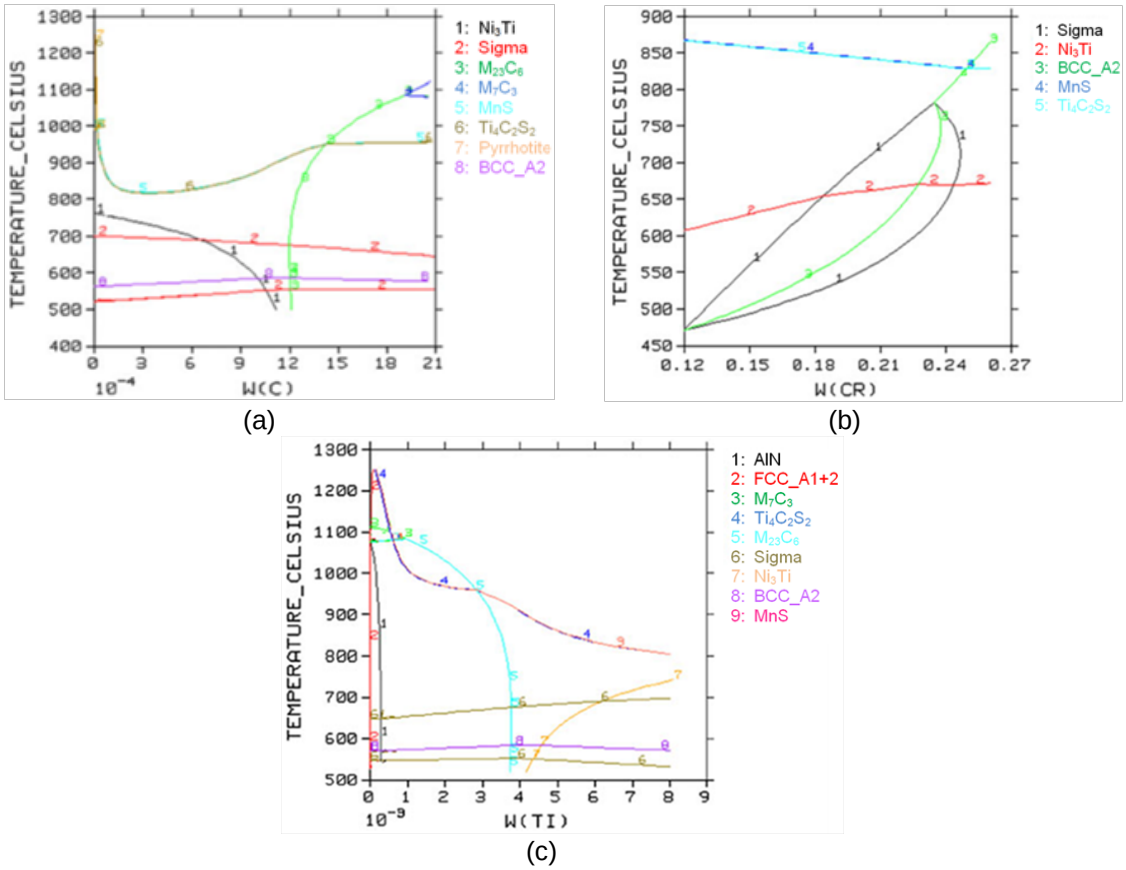

Figure 2-13: (a) Carbon-, (b) Chromium- und (c) Titanium-Isopleth of Alloy 800H [31]

[1] Thermo-Calc and Dictra are programmes of the company Thermo-Calc Software

An equilibrium calculation at a temperature of 1150 ° C resulted in a 10 times higher concentration of niobium and 4 times higher concentration of nitrogen when compared to the matrix at room temperature. **Figure 2-13** shows the thermodynamic calculations assuming a niobium concentration of zero. There occurs in addition to the formation of carbides in Alloy 800H the formation of other compounds, such as manganese sulphide (MnS), titanium carbosulfide ($Ti_4C_2S_2$) and pyrrhotite (consisting of Ti, Mn, S, and other elements). The red lines in Figure 2-13 a limit the area in which the sigma phase occurs. From all three graphs, Figure 2-13 a to c, it is apparent that particularly in this temperature range, there is the possibility of the formation of multiple phases.

2.4 Dislocation structure

Nicolin [29] has shown the development of microstructure in Alloy 800HT based on parameters of dislocation density, particle volume fraction and particle distance. The investigations were carried out on specimens from interrupted creep tests with isothermal heat treatments of 800 °C and 70 MPa and at 900 °C and 45 MPa.

Alloy 800HT is a further development of Alloy 800H for the application in the high temperature range with a corresponding high temperature strength due to carbide precipitations of type $M_{23}C_6$ und Ti(C,N). In **Figure 2-14** the microstructure of Alloy 800HT is shown in the initial state.

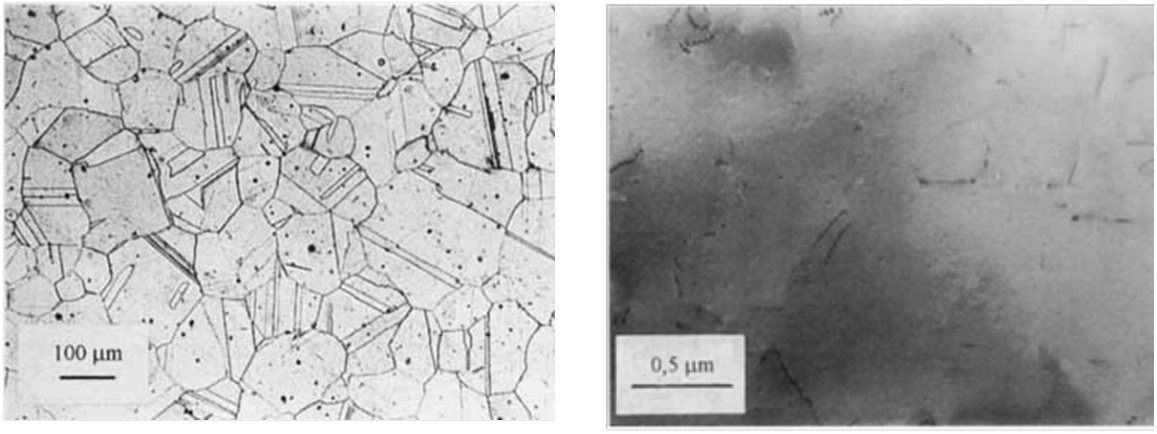

(a) (b)

Figure 2-14: Microstructure of Alloy 800HT in solution annealed state (a) OM, (b) TEM [29]

Compared to Alloy 800 H no difference can be seen in the microstructure based on optical microscopy, see **Figure 2-14 a**, compare with Figure 2-2. The microstructure has 80 microns large grains and isolated twin grains. Furthermore, the carbides solidifying from the melt are mostly inside the grains [29]. On the basis of the investigations carried out by transmission electron microscopy (TEM) (see Figure 2-14 b) it can be seen that there are only few small carbides. At the same time in the almost precipitation-free microstructure, short segments of dislocations are recognizable which serve as nucleation sites for precipitates during creep or thermal stress [29].

Samples after creep loading were investigated. To preserve the microstructure state, the samples were cooled down under load. The creep rupture strength of alloy Alloy 800HT under the respective conditions is shown in **Figure 2-15**.

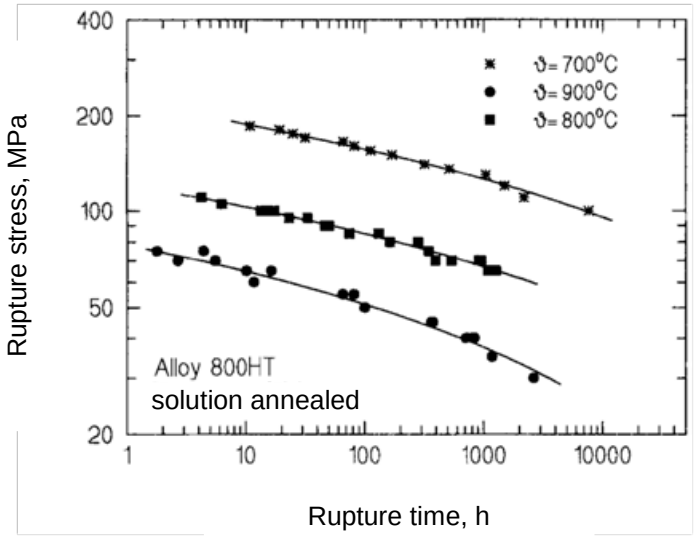

Figure 2-15: Creep rupture strength of Alloy 800HT [29]

According to Nicolin [29], the creep stress rupture times determined here between 185 and 30 MPa agree with values in the literature. Due to excessive ageing caused by the high temperatures, an accelerated precipitation of carbides occurs which results in a more than four orders of magnitude lower creep stress and an increase in the minimum creep rate, compared to the initial state. With increasing stress the difference becomes smaller. The reason for this is that under higher loads the creep deformation process depends primarily on the strength of the matrix. Ultimately, higher stresses cause shorter creep rupture times and higher creep rupture strain.

Regarding the dislocation structure of the creep loaded specimens, the analysed samples are plotted as creep strain curves with temperature and stress values in **Figure 2-16**. The corresponding TEM images are shown respectively in **Figure 2-17**(a) to (d).

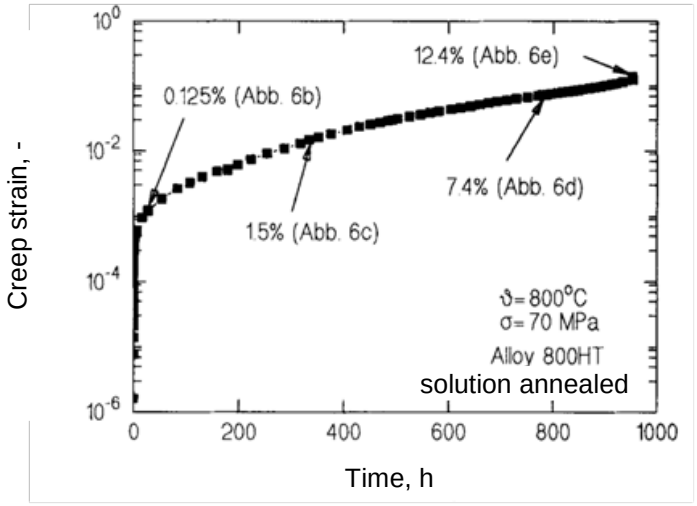

Figure 2-16: Creep strain as function of time at 800 °C / 70 MPa [29]

It can be seen from Figure 2-17 (a) how the dislocation structure in Alloy 800HT is developing with increasing creep strain.

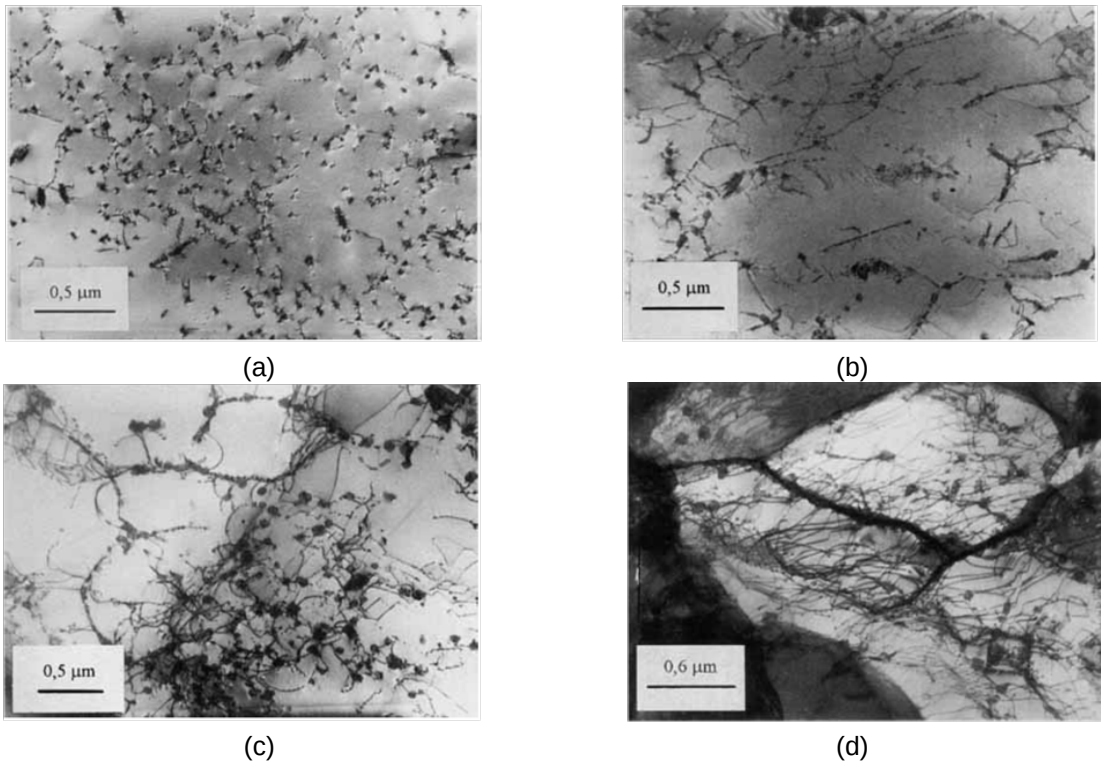

Figure 2-17: Microstructure after creep at 800 °C / 70 MPa, TEM thin foil (a) 0,125 %, (b) 1,5 %, (c) 7,4 %, (d) 12,4 % [29]

After 28 h at 800 °C and a creep strain of ε_k = 0. 125% many small precipitated $M_{23}C_6$ carbides are dispersed with few dislocations. The dislocation density is ρ_v=6,81·10^{+9} cm^{-2}. With increasing load duration and creep deformation the precipitates become coarser. At the same time, the dislocation density increases with slowly growing subgrain structures until finally fracture. At the end of the creep test the dislocation density is ρ_v=8,7·10^{+9} cm^{-2} and the alloy has a distinct subgrain structure.

In **Figure 2-18**, the measured values of the individual test samples are shown graphically.

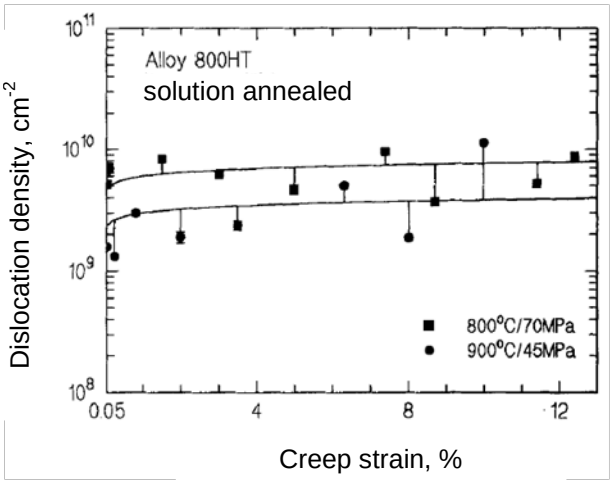

Figure 2-18: Dislocation density ρ_V as function of creep strain for 800 and 900 °C [29]

Comparatively, the dislocation density of tests carried out at 800°C is higher than those obtained at 900°C. Thus strain softening is higher due to longer test periods carried out at 900°C than due to dynamic recovery [29].

By means of the tests performed in [29], it was demonstrated that the hardening effect due to the interactions of carbides with dislocation leads to two different carbide size classes. In addition, the precipitations were delayed due to a superimposed creep load. However, after the precipitation process is finished, a faster coarsening of precipitates occurred in the isothermal condition compared to the creep strained condition. In

this regard **Figure 2-19** shows the middle particle distance as function of stress duration, for creep deformation (70 MPa) and thermal aged state.

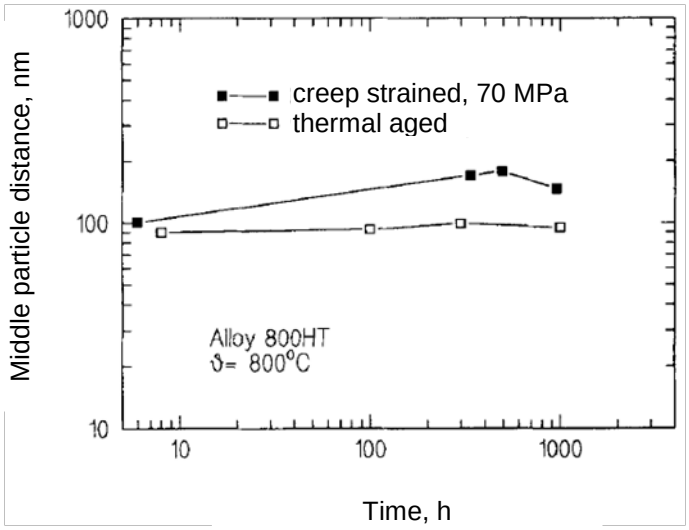

Figure 2-19: Middle particle distance as function of test duration (800 °C) [29]

Clearly visible is the influence of creep load on the precipitation process. The increase before and reduction after the peak show clearly the characteristics of the increase and decrease in diameter of carbide particles due to creep superimposition.

Van Wortel [32] investigated the behaviour of relaxation cracks in Alloy 800H by considering the dislocation density. **Figure 2-20** indicates that the dislocation density increases with increase in hardness due to welding, cold deformation, or cyclic loads.

Consequently in welds which are exposed to high temperatures, precipitations of fine carbides occur on the dislocation nodes, which block dislocations and lead to a further hardening. The studies confirm the precipitation of fine $M_{23}C_6$ carbides at temperatures between 500 and 750 ° C.

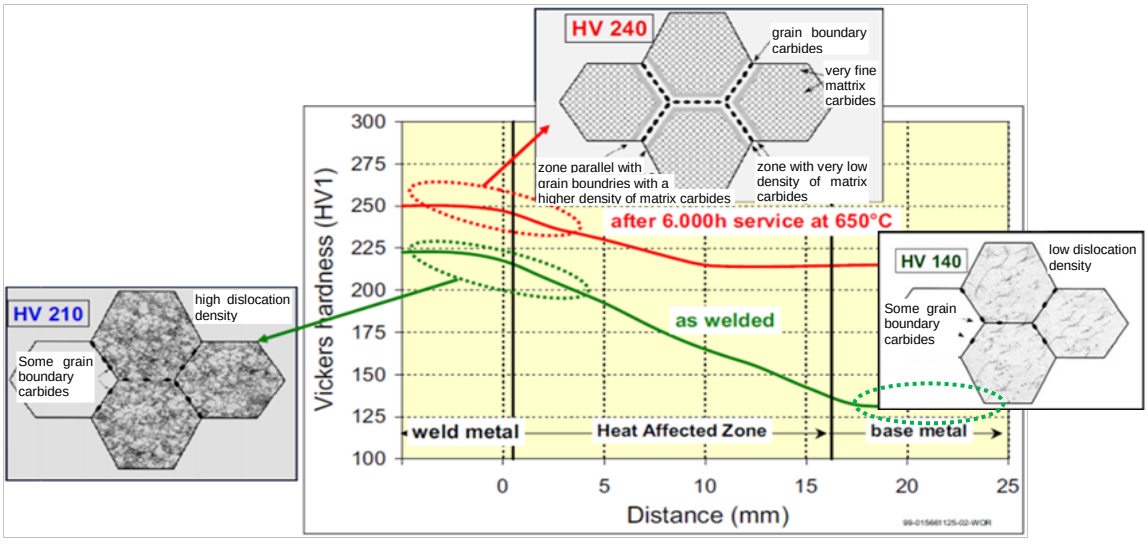

Figure 2-20: Influence of temperature on dislocation density and hardening across the HAZ [32]

Dislocations are able to move as a result of thermal and / or mechanical stress in components. Dislocation creep is based on the climbing of edge dislocations under the condition of an atom space-change in a vacancy mechanism [33]. Climbing of edge dislocations at low and high temperatures differ. Thus for a vacancy diffusion on regular lattice places is required, which is not effective at low temperatures and works only above 0,4 • Ts[2] effectively. Subgrain boundaries result from the climbing operations due to the

[2] absolute melting temperature

rearrangement of dislocations. **Figure 2-21** shows these subgrain boundaries in Alloy 800H after a creep load in the stationary area.

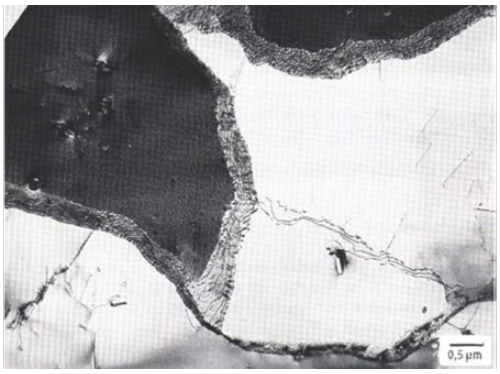

Figure 2-21: Subgrain boundaries in Alloy 800H after creep load [33]

Summary

- *Alloy 800 H is an austenitic Ni-Fe-Cr alloy, which belongs to the group of solid solution hardening materials. The usually as-received condition (solution annealed) shows twin grains and in the austenitic matrix carbon nitrides and chromium carbides are present.*
- *The grain size of Alloy 800 H is from 70 to 180 µm and is of use for the increased creep rupture strength above 600 ° C.*
- *Using a GBE treatment the resistance to grain boundary diffusion can be increased and the strength can be improved at room temperature.*
- *Under the influence of temperature and time Alloy 800H hardening due to the precipitation of secondary chromium rich carbides (M23C6). These are formed in particular on the grain boundaries in the temperature range 550-1100 ° C. The carbides of the type TiC are usually located within the grains and can be found at temperatures above 700°C. Further, there is the possibility of forming a γ 'phase in a temperature range 440 to 650 ° C.*
- *After long-term loading some embrittling intermetallic phases can form such as G and σ-phase as well as Florenskyite (FeTiP)*
- *Alloy 800H shows some precipitations with dislocations in the as delivered state. With increasing stress duration and creep deformation, a coarsening of the precipitates and an increasing dislocation density with slowly increasing subgrain structures could be observed.*

3. Mechanical properties

The operational range of Alloy 800H according to the manufacturer [5] is shown in **Figure 3-1** based on the tensile strength, elongation and yield strength as function of temperature.

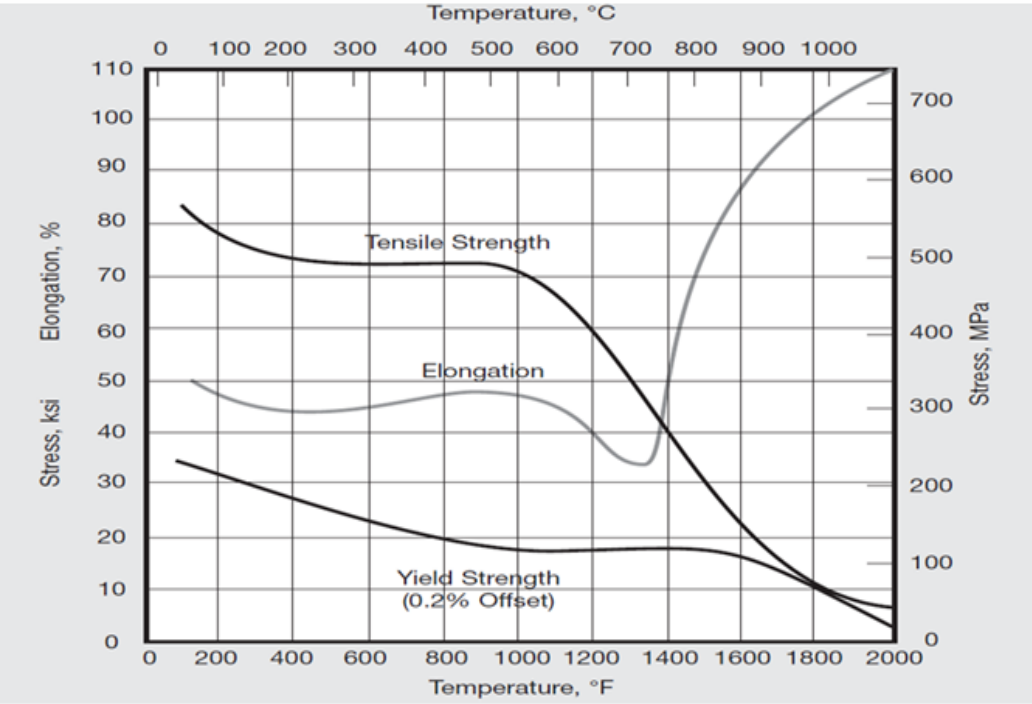

Figure 3-1: Mechanical properties of Alloy 800H [5]

The mechanical properties in the literature [3] of Alloy 800, Alloy 800H and Alloy 800HT at room temperature are compared in **Table 3-1**.

Alloy	Yield Strength MPa	Tensile strength MPa	Elongation %	Reduction of area %	Hardness R_B
800	310	585	40	40	85
800H	275	585	45	40	80
800HT	275	585	40	40	80

Table 3-1: Mechanical properties of Alloy 800 variants at room temperature [3]

Roy [7] measured the mechanical property values of Alloy 800H by means of tensile tests at different temperatures, according to ASTM E 08 specifications. **Figure 3-2** shows the results from experimental stress-strain diagrams.

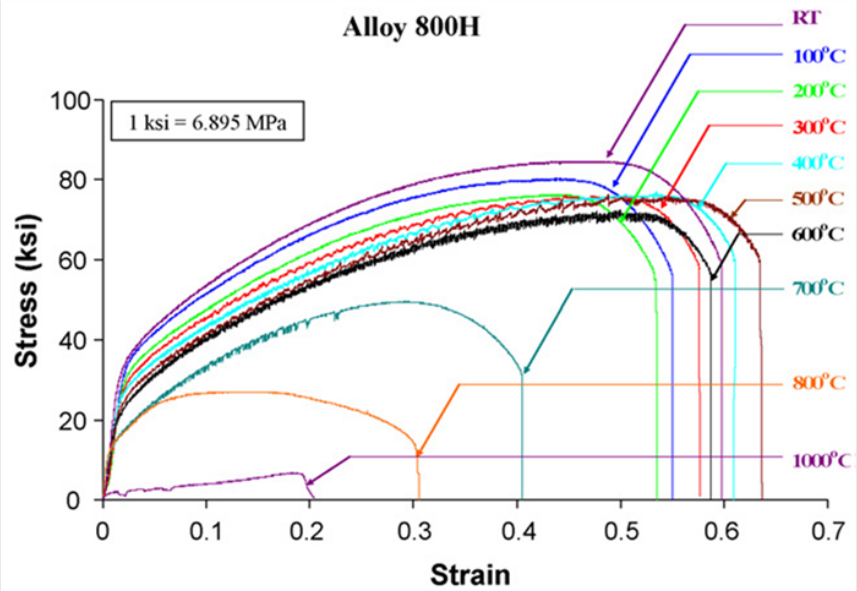

Figure 3-2: Stress-strain diagram of Alloy 800H as function of temperature [7]

The specific values of the stress-strain diagram are listed in **Table 3-2**.

Temperatur °C	Yield Strength MPa	Tensile strength MPa	Elongation %	Reduction of area %
22	261	594	58,5	67,5
100	246	543	53,9	66,3
200	228	523	52,6	64,0
300	213	530	55,0	61,2
400	190	528	60,2	58,9
500	170	526	60,4	57,5
600	151	496	57,6	62,0
700	103	342	39,1	61,6
800	101	184	31,4	60,3
1000	8	46	21,0	10,0

Table 3-2: Material properties of Alloy 800H as function of temperature [7]

In addition to the characteristics of Alloy 800H researched in the literature, internal tests to determine the relaxation behaviour have been carried out at the MPA Stuttgart. The results obtained here are shown in **Figure 3-3**.

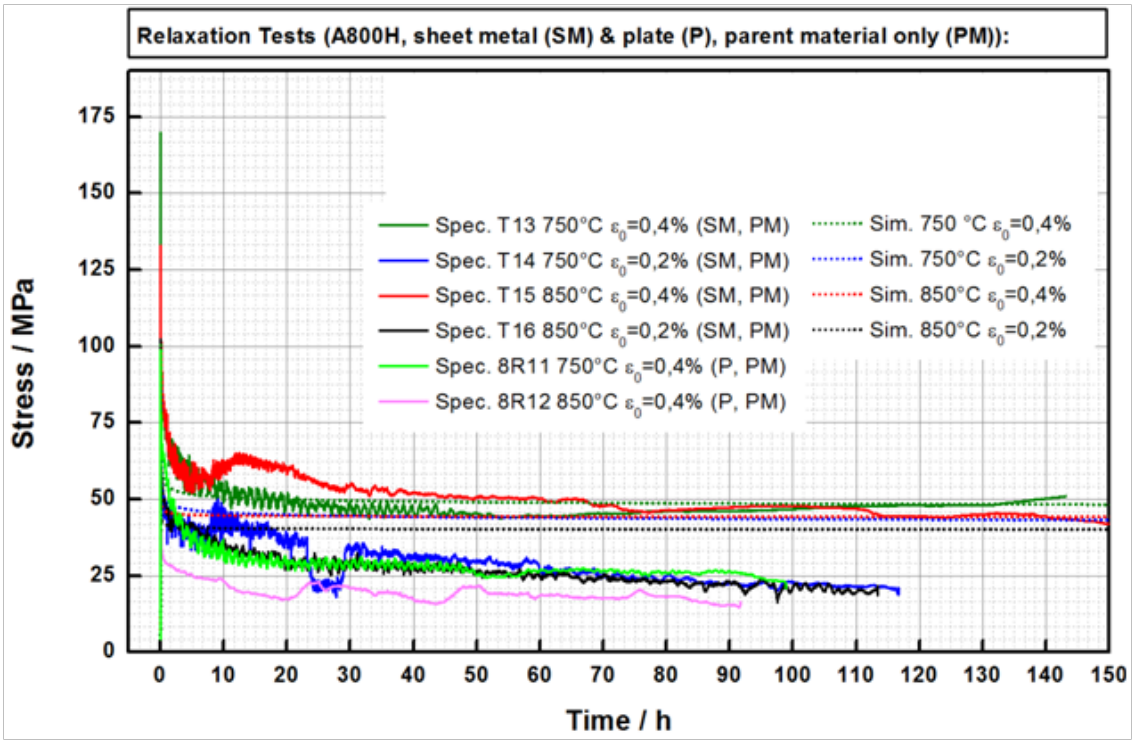

Spec. ~ Specimen, Sim. ~ Simulation

Figure 3-3: Relaxations tests on Alloy 800 H (MPA Stuttgart)

Results given in the literature [34] support the examinations carried out internally. Furthermore the results provide evidence of a precipitation induced contraction of the alloy Alloy 800HT during the investigation time, see **Figure 3-4**.

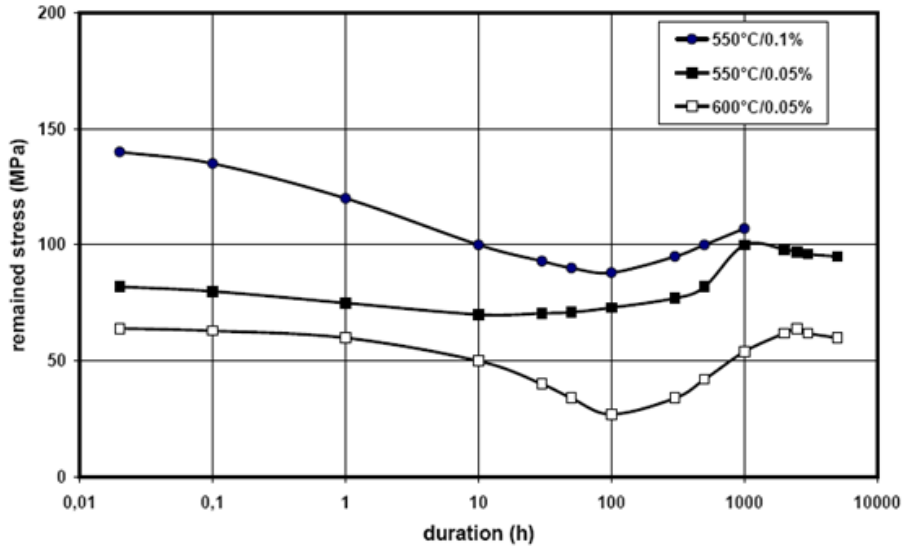

Figure 3-4: Relaxation and contraction of Alloy 800HT at 550 and 600 °C [34]

The contraction occurring is significantly more pronounced at 600 ° C than at 550 ° C. The stress increases after 100 h and reaches values above the maximum starting stress.
Further investigation revealed that a contraction took also place at higher temperatures, 700 to 900 ° C, with a recovery of stress from 40 to 70%, see **Figure 3-5**.

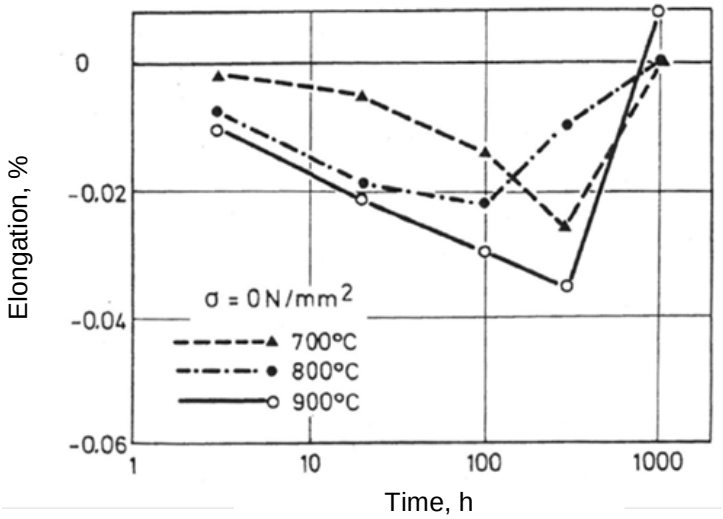

Figure 3-5: Negative creep of Alloy 800HT at 700 to 900 °C [34]

Because of negative creep due to precipitations changes, components should be designed, so that a free contraction is possible during operation.

Summary

- *The mechanical strength characteristics of the alloy provide a yield strength of about 230 MPa at room temperature, a tensile strength of about 590 MPa and a strain to rupture of about 50%.*
- *Depending on the load duration and temperature in Alloy 800HT, a 70% recovery of stress occurs due to a precipitation-induced contraction.*

4. Welding of Alloy 800H

It is important to note for the welding of stainless steels and also Alloy 800H, that the effect of non-rusting is based on the formation of a protective layer, the passive layer, through the influence of atmospheric oxygen. The formation of the passive layer occurs automatically in materials with a Cr content of about 12%. The formation of this passive layer may be hampered by scale, tarnish, weld spatter or weld slag residues [36]. Thus it is necessary to remove these contaminating effects after welding. This can be done mechanically or chemically.

Nickel alloys usually show a very low diffusion rate of alloying elements in the matrix, which leads to rapid cooling and extensive micro-segregations during solidification, particularly at cooling rates in the range of several tens to several hundred °C /s and at short solidification times of 0.01 to 10 seconds [3].

Starting from the ternary solidus projection of the Ni-Fe-Cr system, which indicates that austenite is the only stable phase in nickel-rich alloys, the solidification of weld metals with minor alloying additions also occurs completely austenitic [3].

The addition of aluminium and titanium in welding consumables is used for binding oxygen and nitrogen contamination from the atmosphere. However, the addition of niobium and titanium increases the resistance to crack sensitivity [3]. Due to the presence of carbon, and the simultaneous presence of niobium or titanium the formation of MC carbide takes place in Alloy 800.

Additions of carbon to Fe - Ni - Cr alloys often leads to precipitation of $M_{23}C_6$ type carbides in the solid state during the cooling portion of the weld thermal cycle [3]. This is caused by the decrease of the solubility of carbon in the austenite with decreasing temperature.

4.1. Welding processes

The processes used in the literature [42], [23] for the production of welded joints in Alloy 800H are tungsten inert gas (TIG), metal inert gas (MIG), shielded metal arc (SMAW) and electron beam (EB) welding processes. **Table 4-1** specifies the welding method recommended in the literature related to the grain size of Alloy 800.

	Grain size	MIG	EB	TIG	SMAW
Alloy 800	Coarse [1]	—	—	—	×
	Fine[1]	×	×	×	×

— not suitable, × suitable

[1] fine ~ grain size < ASTM 5, coarse ~ grain size ≥ ASTM 5

Table 4-1: Recommended grain size of the welding process [42]

Furthermore, for the production of an accurate weld seam the viscosity of the melt pool and a lower weld penetration compared to ferritic materials has to be considered. As a result, an elliptical or rounded trailing edge of the melt pool is more effective for minimizing cracks in the weld, because segregations in the centre line of the weld are reduced. Additionally convex instead of concave weld beads are to be preferred, regarding the reduction of cracks in the weld centre line [42].

In [43] the use of plasma, laser beam and TIG welding processes to carry out the weld joint of Alloy 800 H are described. The welded specimens were produced as standard butt welds with a seam length of 200 mm. The wall thickness of the welded test specimens is 3 mm.

The welds have been made automatically by using a clamping and forming device and with the parameters specified in **Table 4-2**.

Alloy 800H	Laser arc welding	Plasma welding	TIG welding
Power P/ Current I	1,5kW	120A	190A
Welding speed v_s	115cm / min	70cm / min	102cm / min
Energy input per unit length E	0,78kJ / mm	2,3kJ / mm	1,98kJ / mm

Table 4-2: Welding parameters of the joining processes [43]

All laser beam welded joints were performed by means of a CO_2 laser. During the welding a mixture of nitrogen and hydrogen (95% N_2 and 5% H_2) and an argon-helium-hydrogen shielding gas (72% Ar, 20% He, 8% H_2) were used for the fabrication [43].

Due to the increasing nickel content of the alloy the importance of a larger cover with protection and forming gases is greater, as only then can a proper seam formation be guaranteed. At the same time the welding speed must be reduced with increasing nickel content. This is due to the viscosity of the melt pool which increases with increasing nickel content [43].

In comparison to the plasma and TIG process, the laser beam method has the lowest heat input because of the high welding speed and low arc energy. Consequently a low thermal distortion and low residual stresses are to be expected.

Figure 4-1 shows the metallographic analyses of the weld seams carried out for the respective joining processes. The images reveal that a greater grain coarsening is visible in the plasma process compared with the laser beam and TIG processes. The weld metal shows a dendritic structure with embedded carbide precipitations. A significant vertical centre line through the melt fronts can be observed in the seam produced by laser beam process.

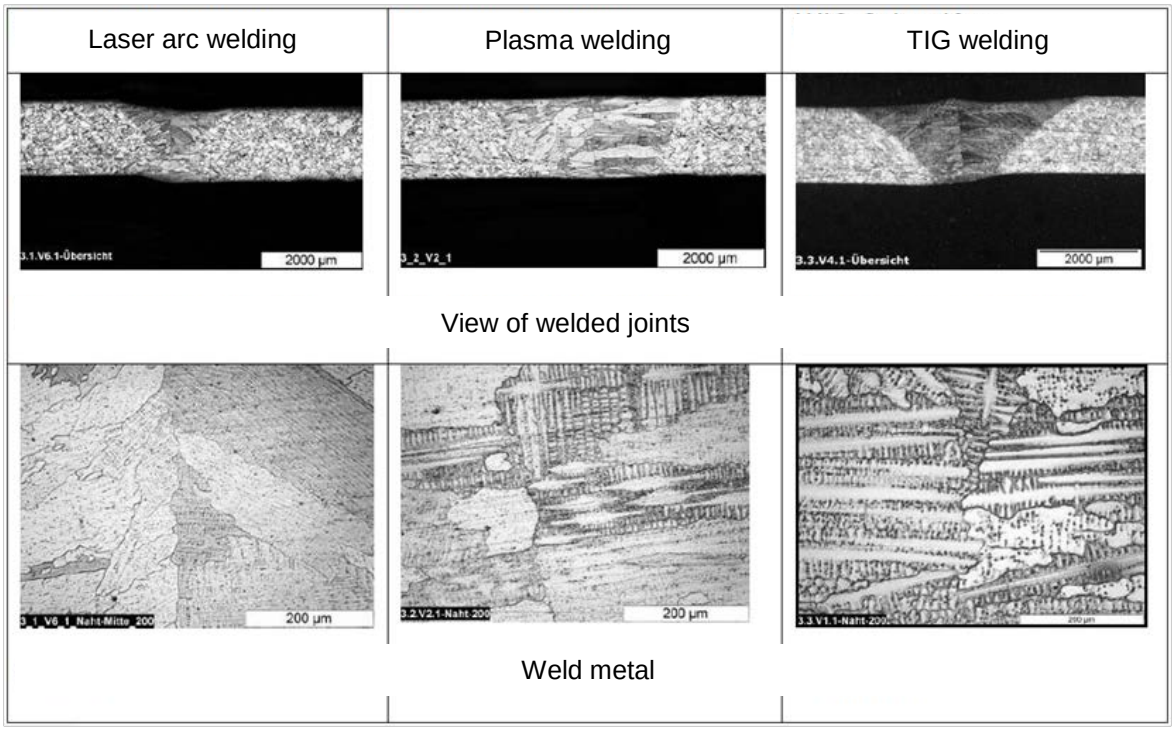

Figure 4-1: Macro- and microsections of weld joints of Alloy 800H [43]

The weld seam produced by the laser welding method has the finest grain size due to the high cooling rate in this case [43].

It could be demonstrated that no hot cracks occurred in the welds fabricated in accordance with the conditions set out.

The findings obtained by this research [43] can be used for all thin-walled steel structures subjected to a cyclic high temperature operation subjected to exposure to aggressive media. This includes besides reformer systems being considered, also high temperature heat transfer systems which in general are subjected to an increasing material loads in order to improve efficiency by downsizing and process intensification.

In addition Mizia [31] describes the diffusion welding of Alloy 800H as a method for the production of components in the aerospace and nuclear industries, by which all physical, mechanical and metallurgical phenomena can be influenced such as: control of grain growth and crystallographic texture of the weld transition, diffusion processes and phase transitions with different concentration profiles of the various components and precipitates, and the prevention of high-temperature oxidation of various components (especially chromium).

4.2. Welding parameters

For processing and welding of stainless and heat-resistant steels, there exist general welding technical guidelines according to the DVS sheet 0912 [44]. Thus, a possible maximum corrosion and oxidation resistance exists only when no external impurities are present. Therefore in order to avoid corrosion damage the workplace has to be clearly separated from those in which the conventional carbon steel is processed, for example by partition walls. The necessary cleaning of the base material and the filler metal should be done only with acetone. Detergent based on chlorinated hydrocarbons, such as perchloroethylene (PER), lead to the formation of highly toxic phosgene under the influence of UV radiation which occurs during welding [36].

During the preparation of weld seams with a possible required grinding process, it must be ensured that no overheating occurs. Regarding the seam spacing and opening angles it must be taken into account that thermal expansion coefficient is up to 50% higher for austenitic steels and thermal conductivity is lower by a third in comparison to ferritic materials. Due to a tendency for warpage the manufacturers of semi-finished products recommend wider root gaps and openings as well as shorter tacking distances. Furthermore, opening angles of about 60-70° are recommended due to the more viscous behaviour of the melt of austenitic materials which reduce shrinkage.

Tack welds which cannot be melted completely during welding must previously be mechanically worked. In addition, when a surface treatment of the root of components under corrosive load is not possible after welding, the tack welding should be carried out with forming gas. The filler and cover layers are to be formed as a stringer beads and with a layer structure as shown in **Figure 4-2**.

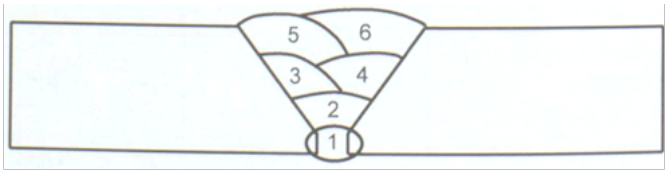

Figure 4-2: Layer structure of a V-seam, thickness of sheet 10 mm [36]

It should be noted that the welding of the root can be done principally as MAG welding. If a high-quality root is required and counter welding of the root is not possible, the TIG procedure is recommended for use in this case [36].

The "German Welding Society (DVS)" also gives recommendations for the use of filler materials. The DVS information sheet 0931 includes metal active gas (MAG) welding of stainless and heat-resistant steels. The filler materials for Alloy 800H and Alloy 800HT are listed in **Table 4-3**

Alloy specification acc. to DIN EN 10088 / DIN EN 10095 / DIN EN 10028-7			Filler materials		
Shortname	W. -Nr.	ASTM / AISI / SAE / UNS	Specification acc. to DIN EN ISO 14343-A / DIN EN ISO 18274	W. -Nr.	AWS A 5.9 / A 5.14
X5NiCrAlTi31-20	1.4958	N 08810	S Ni6082 (NiCr20Mn3Nb)	2.4806	ER NiCr-3
X8NiCrAlTi32-21	1.4959	N 08811	S Ni6082 (NiCr20Mn3Nb)	2.4806	ER NiCr-3

Table 4-3: MAG Filler materials accordingto DVS [36]

For arc welding the appropriate electrodes are listed in the DVS information sheet 0941 [45].

Alloy specification acc. to DIN EN 10088 / DIN EN 10095 / DIN EN 1216 / DIN EN 10269			Filler materials		
Shortname	W. -Nr.	ASTM / AISI / SAE / UNS	Specification acc. to DIN EN ISO 17633-A / DIN EN ISO 14172	W. -Nr.	AWS A 5.9 / A 5.14
X10NiCrAlTi32-21	1.4876	N 08800	Type T NiCr20Mn3Nb	~2.4806	ER NiCr-3 / ER NiCr-3T

Table 4-4: Electrodes for the arc welding according to DVS [45]

Filler materials recommended in the literature [3] and their purpose are listed in **Table 4-5**. Filler materials for Ni-Fe-Cr alloys including 800 and 800 H are preferably based on nickel to achieve welding properties which correspond to the basic material or exceed them. For example, Alloy 800H is welded with the filler Ni-Cr-Co-Mo. Thus the creep rupture strength above 870°C can be exceeded [3].

Filler material	Main purpose
ERNiCr-3 (2.4806)	• Alloy 800, 800H and 800HT for operation-temperatures up to 850 °C • dissimilar welds between steel and nickel base alloys
E/ERNiCrCoMo-1 (2.4627)	• welds of Alloy 800H and 800HT for operation-temperatures between 760 and 1150 °C

Table 4-5: Recommended filler materials in the literature and their purpose [3]

In addition to recommendations from the literature and associations, manufacturers of semi-finished products offer also appropriate filler materials for processing. The nickel base alloys *Nicrofer®3220 H* and *HP* [3] (alloy 800 H and HT) are weldable for all conventional welding processes (TIG, plasma, SMAW, MSG) specified by the manufacturer [2]. The filler materials recommended by the manufacturer are listed in **Table 4-6**.

[3] Nicrofer is a registered trademark by ThyssenKrupp AG

	Filler materials for Alloy 800H and Alloy 800HT		Alternative for Alloy 800HT	
Specification	Wire electrode	Covered stick electrodes	Wire electrode	Covered stick electrodes
Material No.	2.4806	2.4648	2.4627	2.4628
Short name	SG/UP-NiCr20Nb	EL-NiCr19Nb	SG-NiCr22Co12Mo	EL-NiCr21Co12Mo
AWS	A5.14 ERNiCr-3	A5.11 ENiCrFe-3 mod.	A5.14 ERNiCoMo-1	A5.11 ENiCrMo-1

Table 4-6: Manufacturer information of usable filler materials for alloys *Nicrofer®3220 H and HP* (Alloy 800H and HT) [2]

The chemical compositions of the filler materials are listed in **Table 4-7**.

Filler material		Ni	Cr	Fe	C	Mn	Si	Cu	Al	Ti	Co	Mo	Nb	W	S
2.4806 ~2.4648	min.	67	18	–	–	2,5	–	–	–	–	–	–	2,0	–	–
	max.	Rest	22	3,0	0,10	3,5	0,5	0,5	–	0,7	–	–	3,0	–	0,03
2.4627 ~2.4628	min.	44	20	–	0,05	–	–	–	0,8	–	10	8	–	–	–
	max.	Rest	24	3,0	0,15	1,0	1,0	0,5	1,5	0,6	15	10	–	0,5	0,03

Table 4-7: Chemical compositions of filler materials in wt-% [46]

The DVS makes only general statements on which inert gases should be used for MAG welding. For solid and metal (powder) cored wires it is preferable to use of mixed gases of group M1 according to DIN EN ISO 14175, see **Table 4-8**.

Main group acc. to DIN EN ISO 14175	Sub group	Composition				
		CO_2 [%]	O_2 [%]	He [%]	H_2 [%]	Ar [%]
M1	1	0,5 - 5	–	–	0,5 - 5	Rest
	2	0,5 - 5	–	–		Rest
	3	–	0,5 - 3	–		Rest
	4	0,5 - 5	0,5 - 3	–		Rest

Table 4-8: Mixed gases according to DVS [36]

According to information provided by the DVS [36] for the nickel base Alloy 800H [3], a low heat input and interpass temperature of 120°C max are required for an welding of semi-finished products. With regard to the parameters of heat input, interpass temperature and preheating temperature, attention has to be given to information from the materials or filler manufacturer.

The heat inputs for Alloy 800H specified by the manufacturer of semi-finished products are listed as reference values for the welding processes in **Table 4-9**.

Welding process	Energy input per unit length [kJ / cm]	Welding process	Energy input per unit length [kJ / cm]
TIG Manual, fully mechanised	max. 8	SMAW	max. 7
TIG hot wire welding	max. 6	SAW	max. 10
Manual, fully mechanised	max. 10	Plasma	max. 10 – 15*

* depending on the wall thickness

Table 4-9: Energy input per unit length from manufacturer information for material Nicrofer®3220 H and HP (Alloy 800H and HT) [2]

The heat input Q depends on the welding process and the resulting thermal energy. The heat input Q is calculated using the following equation:

$$Q = \eta \cdot E \tag{4.1}$$

Where η represents the relative thermal efficiency of the process and E the energy input per unit length and is given as:

$$E = \frac{U \cdot I}{v} \tag{4.2}$$

with the variables

E: energy input per unit length
U: arc voltage
I: welding current
v: welding speed.

The thermal efficiency η varies, depending on the process, and can be taken from **Table 4-10**.

Process	Thermal efficiency η
Submerged arc welding (SAW)	1,0
Manual arc welding with rod electrode	0,8
Metal active gas welding (MAG)	0,8
Metal inert gas welding (MIG)	0,8
Tungsten inert gas welding (TIG)	0,6

Table 4-10: Thermal efficiency η [49]

A too high heat input leads to negative influences such as:

- Increased distortion and residual stresses
- Undesirable precipitates
- Loss of toughness due to grain coarsening
- Formation of hot cracks
- Increased susceptibility to intergranular corrosion
- Strong secondary oxidation

Thus the heat input should in principle be limited [36]. A reduction of the heat input is performed by increasing the welding speed, lowering of the arc performance (current, voltage) and use of thinner electrodes.

Furthermore, preheating of austenitic steels is not normally carried out. DVS information sheet 0931 [38] explicitly states that completely austenitic materials susceptible to hot cracks and nickel base materials should not be preheated.

4.3. Selected behaviour of Alloy 800 H welds

Lundin [37] examined the softening behaviour of the heat-affected zone (HAZ) in welded joints of Alloy 800 H. The manufacture of the weld samples was based on the parameters listed in **Table 4-11**.

Procedure	Tungsten inert gas welding
Current	100 A
Voltage	12 V
Welding speed	4,23 mm/s (10 ipm)
Protective gas	Argon – 0,85 m^3/h (30 cfh) (10 s pre- and after-flushing of the weld)
Electrode	2 % Thorium-Tungsten-electrode
Arc length	1,6 mm (0,062 inch)
Polarity	Direct current, elektrode negative poled
Interpass temperature	22 °C

Table 4-11: Welding parameters in the test samples [37]

In addition, the welding samples with different heat inputs (28 and 45 kJ/in)[4] were produced. All samples were aged at 700 ° C for 1, 10, 100 and 1000 hours and then analysed.

A softening of the HAZ could be determined for all investigated weld samples. Generally it was found that the width of the softened zone increases with increasing temperature and the minimum hardness of this softened zone increases with increasing ageing time. The hardness profiles obtained are shown in **Figure 4-3** and **Figure 4-4** [37].

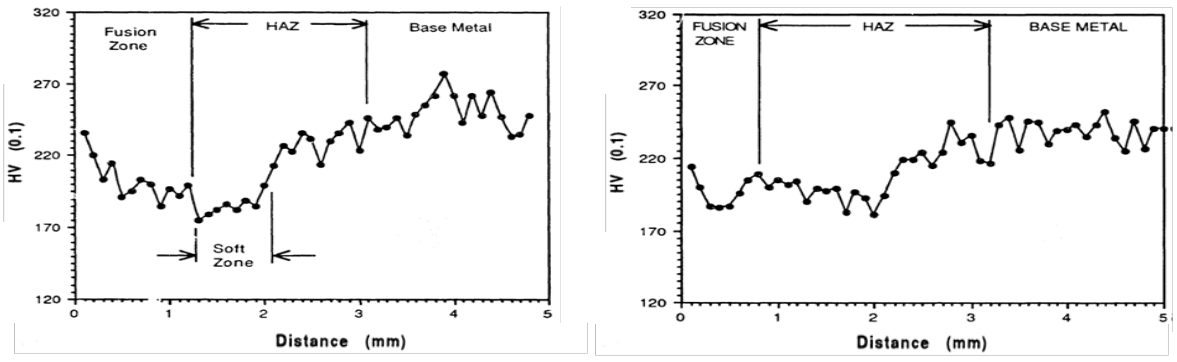

(a) (b)

Figure 4-3: Hardness profile of the WIG-weld in pure welded condition, (a) heat input 28 kJ / in and (b) heat input 45 kJ / from [37]

By comparing [37] the as-welded specimens with the annealed samples it can be seen that in particular the samples aged at 700°C for 1000 hours show significantly more precipitations. This suggests that through heat treatment after welding or by appropriate operating temperatures the softened areas arising from the carbide dissolution during the welding disappear.

[4] ~ 71.1 and 114.3 kJ/cm

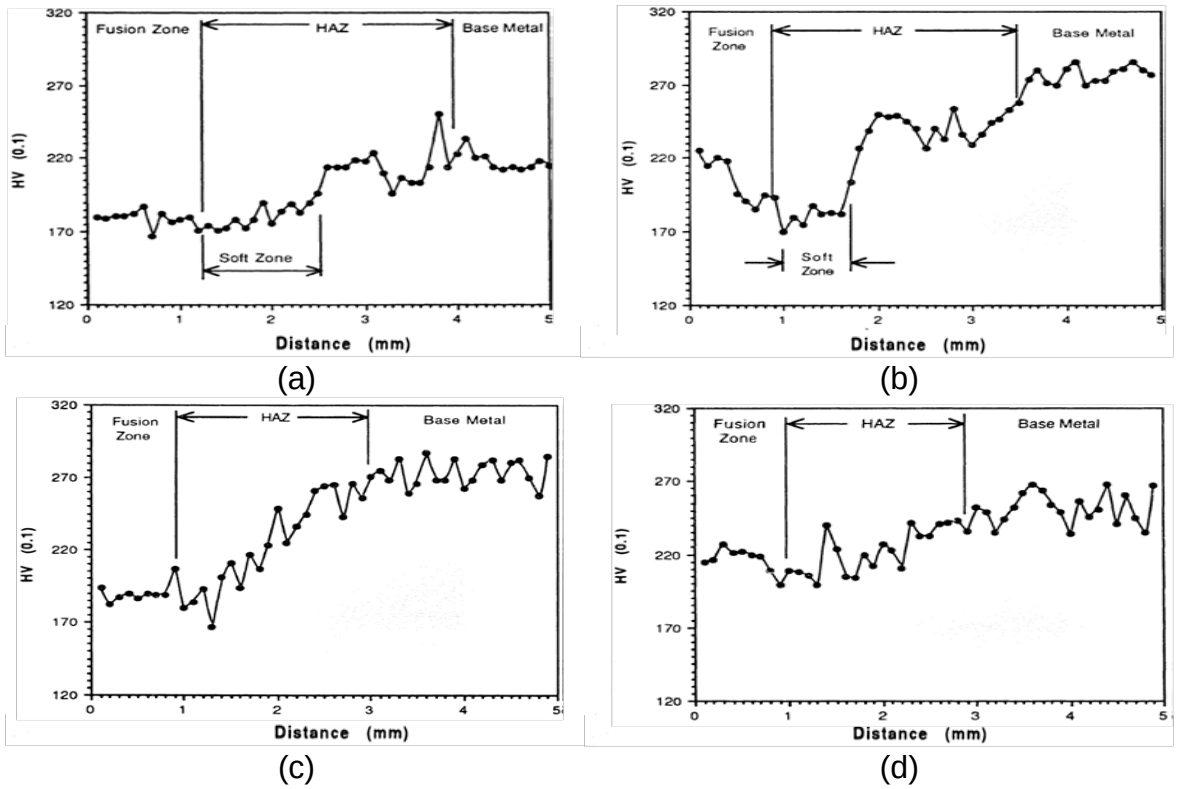

Figure 4-4: Hardness profile of the WIG-weld with a heat treatment 28 kJ/in (a) after 1 h at 700°C, (b) after 10 h at 700°C, (c) after 100 h at 700°C, (d) after 1000 h at 700°C [37]

The precipitations occurring in the test samples are metal carbides (MC with Nb and Ti), nitrides and carbon nitrides and chromium-rich mixed carbides ($M_{23}C_6$). The metal carbides, nitrides and carbon nitrides are more stable during ageing than the mixed carbides [37].

Siresha [38] investigated in his research project dissimilar welds, in particular welded joints of 12 mm thick plates of austenitic alloy 316LN and Alloy 800 materials. The objective was the optimisation of the of transition pieces and filler materials. The base materials and filler materials with chemical compositions used here are listed in **Table 4-12**.

The filer materials 316 and INCONEL 182 were used as electrodes in manual arc welding process and 16-8-2 and INCONEL 82 filler were added as filler wires in the tungsten inert gas welding process. To analyse possible precipitates in the weld seams all samples were annealed at 750 ° C for 100 h

The microstructure resulting from the investigations [38] at the interface between the base material of Alloy 800 and the filler INCONEL 82 and 316 is shown in **Figure 4-5**.

	Base material		Filler material			
Elements	316LN	Alloy 800	316[5]	16-8-2[6]	INCONEL* 182 [7]	INCONEL* 82 [8]
C	0,02	0,09	0,052	0,07	0,05	0,015
Si	0,3	0,7	0,6	–	0,5	0,1
Mn	1,8	1,0	1,7	1,5	7,0	2,8
Ni	12,1	31,8	11,5	8,8	69,0	72,6
Cr	17,9	19,9	18,6	16,2	15,0	19,6
Mo	2,4	–	2,2	1,6	–	–
Ti	–	0,36	0,04	–	0,1	0,37
Nb	–	–	0,01	–	2,0	2,68
Fe	Rest	Rest	Rest	Rest	Rest	Rest

* INCONEL is a registered trademark of Special Metals Corporation

Table 4-12: Chemical composition of the materials wt.-% [38]

It is apparent that in Figure 4-5 a, the interface structure is sharp and an unmixed zone is present, whereas in Figure 4-5 (b) the connection with the filler material 316 has a much wider unmixed transition zone. This is due to the larger difference in chemical composition between filler 316 and Alloy 800 compared to those of INCONEL 82 and Alloy 800 [38].

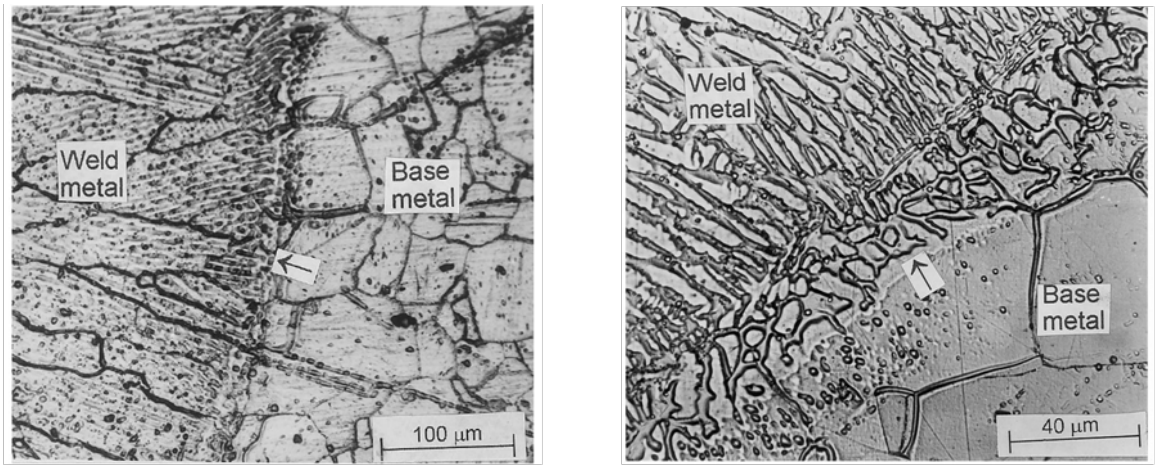

Figure 4-5: (a) Transition zone between filler INCONEL 82 and base material Alloy 800, (b) Transition zone between filler 316 and base material Alloy 800 [38]

At the same time it is evident that the transition zone in Figure 4-5 b shows a grain coarsening. These unmixed or partially mixed zones are due to the formation of a higher melting point [38]. The melting point of the base material Alloy 800 is higher than that of the filler materials so that the convection current is not sufficient for the required flow and mixing. Resulting from this, it is clear that the melting point of Alloy 800 and its composition are closer to the filler material INCONEL 82. Thus a wide unmixed zone cannot be formed and the convection in the weld pool ensures the formation of a thin laminar unmixed layer.

[5] W.Nr. 1.4401, UNS W31610, AWS A5.4, E 316
[6] W.Nr. - , UNS S16880, AWS A 5.9, ER16-8-2
[7] W.Nr. 2.4807, UNS W86182, AWS A5.11, ENiCrFe-3
[8] W.Nr. 2.4806, UNS N06082, AWS A5.14, ERNiCr3

In the filler materials 316 and 16-8-2 a discontinuous network of sigma phase occurred after ageing. Compared to filler 16-8-2, filler 316 shows a stronger sigma phase formation due to the higher chromium and molybdenum content. The filler INCONEL 182 does not show precipitations of sigma phase under the ageing parameters present here. Further studies [38] revealed that precipitations of sigma phase occurred in INCONEL 182 at temperatures between 700 and 900 ° C and by annealing at 700 ° C for 10,000 hours.

The use of flux-covered INCONEL electrodes showed a greater number of inclusions than using process by inert gas. The higher content of inclusions led to a ductility and toughness reduction. However, the INCONEL filler metals showed a higher metallurgical stability in terms of ageing with an induced formation of sigma phase [39].

Additional studies show an almost identical thermal expansion coefficient between the base material Alloy 800 and the filler metal INCONEL 82 [38]. **Figure 4-6** shows the filler metals with their measured coefficients of thermal expansion.

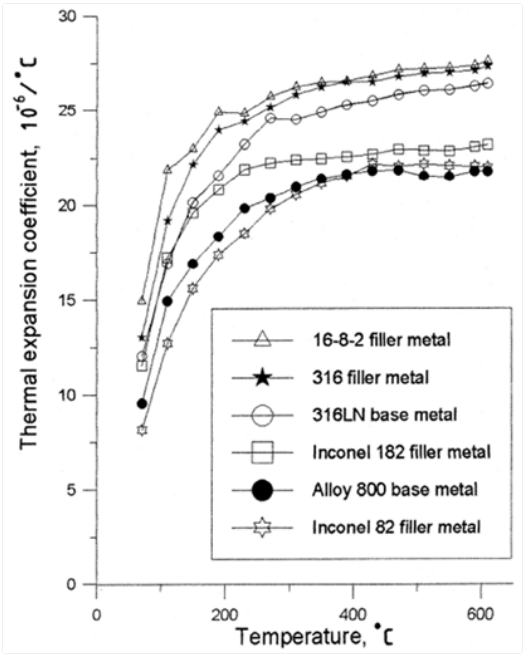

Figure 4-6: Thermal expansion coefficient of filler materials and of base material Alloy 800 [38]

Siresha [40] examined in a further study welded joints between ferritic and austenitic steels, designed to operate at 550 °C and a lifetime of about 200 000 hours. The thickness of the samples of Alloy 800 used here is 12 mm, solution annealed and grade 91, normalised at 1080 °C and annealed at 750 °C for 1 h. For the joints the nickel-based filler materials INCONEL 82 and INCONEL 182 are used. INCONEL 82 was used a welding wire for the root pass using the TIG welding process and INCONEL 182 as electrodes for the subsequent weld layers by means of arc hand welding. The preheating and interpass temperature was 250° C. Due to the martensite formation of grade 91 and the necessary annealing, the weld samples were subjected to an additional heat treatment at 760 °C for 2 hours [40]. After welding the samples were annealed at a temperature of 650 °C and a duration of 200, 500, 2000 and 5000 hours.

The investigations show that the HAZ of Alloy 800 has a distinctive grain growth with a subsequent recrystallisation due to the high heat input during welding. Furthermore, it can be seen that most of the pre-existing precipitates in the base material are dissolved and new precipitates are caused only due to the cooling along the grain boundaries. Consequently the tempering after welding has no significant effect on the HAZ in Alloy 800 [40].

The measured Vickers hardness across the weld seam in the various states of ageing is shown in **Figure 4-7**. The annealing conducted at a temperature of 650 °C for 200 and 500 hours causes a small change in hardness along the seam. It is clearly seen that the hardness particularly in the filler metal and in Alloy 800 increases significantly during annealing of 2,000 and 5,000 hours due of precipitation reactions [40].

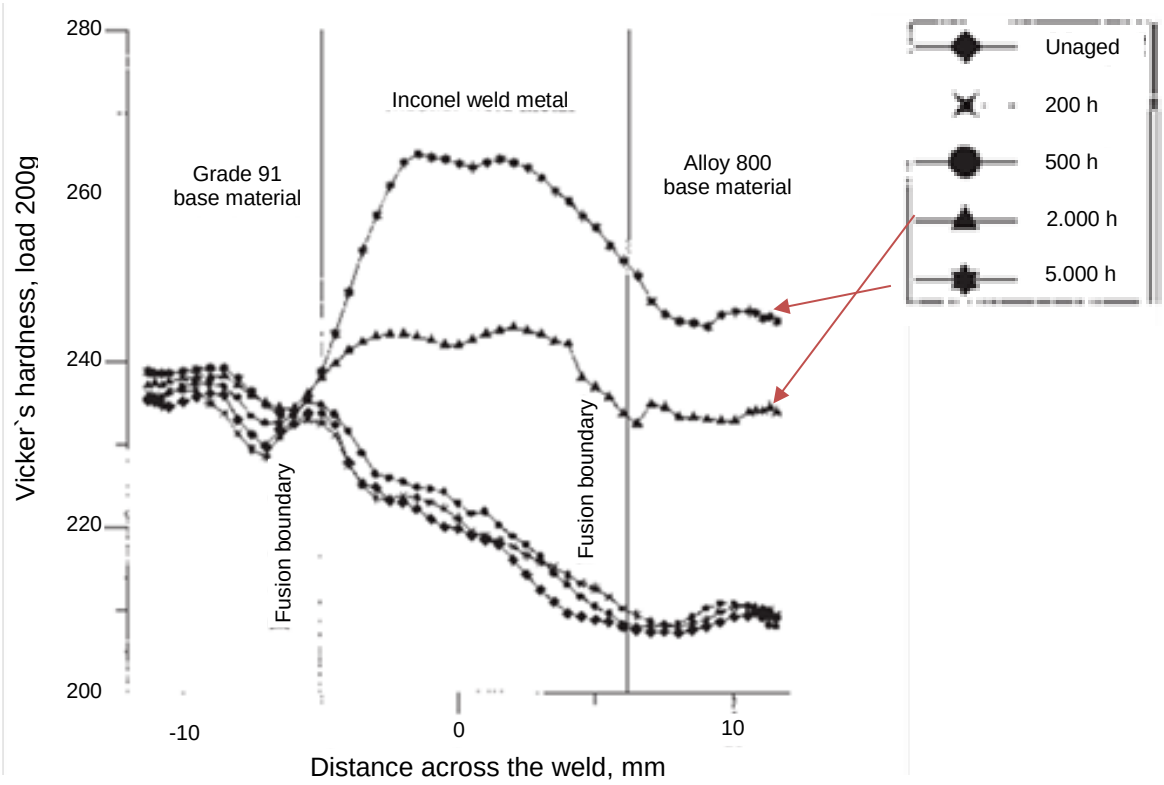

Figure 4-7: Hardness profile across the entire weld seam of the un-aged and differently aged samples [40]

The performed tensile tests on welded joint specimens showed, with the exception of the pure welds and the joints annealed after welding which were tested at room temperature, that all other joints failed in the ferritic base metal (Grade 91), far from the weld seam [40].

The tests of welded joints at 550 °C show a reduction of the yield strength and a slightly lower tensile strength compared to the one at room temperature. Thus, it cannot be assumed that there is an increase in ductility at temperatures up to 550 °C.

Additionally notch-bar impact tests at room temperature were carried out on weld seams in the welded, tempered and in the aged condition, as well as on the two base materials. Through annealing a slight increase of toughness can also be seen, due to the slight increase in ductility. The toughness of the weld joints is below the base materials and shows a drop up to ca. The non-aged filler metal shows a ductile fracture with a large number of small pits without any precipitations, the filler metal aged after 5,000 h shows a mixed fracture surface with single cleavage fracture faces with precipitations in the middle range of ductile fracture.

The phases precipitated in the HAZ were identified as Ni_3Ti, $M_{23}C_6$ and NbC, whereas NbC is caused only by the filler metal. At the same time these precipitates were formed under prolonged thermal load in Alloy 800. These precipitation reactions are responsible for the increase in hardness after 2000 and 5000 hours of ageing, see **Figure 4-7**. Furthermore, dislocation movement is reduced due to these precipitations, which explains the decrease of toughness in the filler metal during the thermal load at 625 °C.

Schubert [34] carried out an assessment of the creep rupture strength of different welded joints of Alloy800. The creep rupture strength is dependent on the base material variant (Alloy 800 and Alloy 800HT), the filler material and the temperature. The welding procedures and filler materials used are listed in **Table 4-13**.

Welding process	Filler materials	Comment
Manual arc welding	• EZ 21 33 B (≈1.4850) • EL-NiCr16FeMn (2.4620) • ≈EL-NiCr19Nb (≈2.4648) • EL-NiCr20Mo9Nb (2.4621) • EL-NiCr21Co12Mo (2.4628)	almost similar filler material IN 112 almost similar filler material for Alloy 617
MIG-Impulse	• S-NiCr20Mn3Nb (2.4806) • SG-NiCr21Mo9Nb (2.4831) • SG-NiCr22Co12Mo (2.4627)	almost similar filler material for Alloy 617
TIG	• W/GZ 21 33 Mn Nb (≈1.4850) • S-NiCr20Mn3Nb (2.4806) • SG-NiCr21Mo9Nb (2.4831)	almost similar filler material
TIG-impulse	• S-NiCr20Mn3Nb (2.4806)	

Table 4-13: Welding procedure and filler materials used [34]

The weld strength factor (WSF) is usually used for the assessment of the lifetime of components with welded joints. The WSF is shown in equation 4.3 and represents the ratio of the creep-rupture strength of the welded joint $R_{m(w)/t/T}$ to the creep rupture strength of the base material $R_{m/t/T}$. :

$$WSF(t,T) = \frac{R_{m(w)/t/T}}{R_{m/t/T}} \quad (4.3)$$

The creep rupture strengths to be considered are determined at same time t and same temperature T [41].

The weld strength factors determined in the investigations for the creep rupture strength at 10^5 h are listed in **Table 4-14** as functions of temperature and filler material.

Base material	WSF	600 °C	650 °C	700 °C	750 °C	800 °C	850 °C	900 °C	950 °C	1000 °C
Alloy 800 H +AT*	1.4850 2.4627	1	1	1	1	1	0,95	0,9	0,85	0,8
	2.4648 2.4806 2.4621 2.4831	–	1	0,95	0,85	0,75	0,7	0,65	0,63	0,6
	2.4620	1	1	0,95	0,85	0,75	0,55	0,3	–	–
Alloy 800 HT +AT*	1.4850	1	1	0,95	0,9	0,8	0,7	0,6	0,5	0,4
	2.4806 2.4621 2.4831	1	1	0,9	0,8	0,7	0,6	0,5	0,4	0,3
	2.4620	1	1	0,85	0,75	0,65	0,55	0,45	0,3	–

* +AT –solution annealed condition

Table 4-14: Weld strength factors [34]

The smallest welding reduction occurs [34] using similar weld filler materials.

The weakest point of welded joints of solution annealed Alloy 800 is the base material up to an operation temperature of ca. 700°C, while at temperatures between 700 and 800°C it is the heat-affected zone, and above 800°C the weld metal.

Summary

- *With regard to the manufacture of welded joints made of alloy 800 H welding processes considered are in particular gas shielded metal arc welding, tungsten inert gas welding and manual arc welding. In addition, special procedures such as tungsten plasma welding, diffusion welding, laser and electron beam welding are used.*
- *For the welding of Alloy 800H processing instructions of stainless steels (removal of scale, heat tinting, spatter and weld slag residues) and of the austenitic steels (viscous melt pool, low thermal conductivity, high thermal expansion) must be considered.*

- *To reduce micro-segregations during solidification accompanying elements such as sulphur are to be avoided.*
- *The filler metal 2.4806 is consistently recommended for the production of welded joints by associations and manufacturers of semi-finished products and in the literature. This filler metal has a nearly identical thermal expansion coefficient as Alloy 800H.*
- *Heat input and energy input per unit length must be kept low and a maximum interpass temperature of 120 °C should be maintained. Depending on the welding process, the reference values of the energy input per unit length are between 6 to 15 kJ / cm.*
- *The high heat input during welding (28 and 45 kJ / in) leads to a softening of the HAZ due to carbide dissolution, whereby during a post weld heat treatment or at appropriate operation temperatures (700°C) a re-precipitation occurs and the softened zones disappear.*
- *The weld strength factors for different welded joint in the temperature range from 600 °C to 1000 °C are available.*

5. Crack phenomena

5.1. Hot cracks

Basically there are two types of hot cracks. Type I includes the segregation induced cracks (solidification and liquation cracks) whereas Type II contains cracks due to a drop in the deformation capacity (Ductility Dip Cracks (DDC)) [50].

The information sheet DVS 1004-1 [51] defines hot cracks as phenomena caused in the presence of low-melting, brittle substances on the grain boundaries and caused by high temperatures during or after completion of the welding process.

The factors which influence hot cracking during welding are unfavourable interactions between metallurgical, constructional and technological conditions.

The influencing parameters here are the alloy composition, the nature of the primary crystallisation, the amount of impurities, low-melting eutectics, the welding parameters and the resulting heat transfer, material thickness with welding stresses and deformations.

According to [43] for the production of a welded joint of hot crack susceptible materials, it is necessary to comply with the recommended energy input per unit length and have material surfaces which are free of scale, grease and oil.

The different types of hot cracks are shown schematically in **Figure 5-1**.

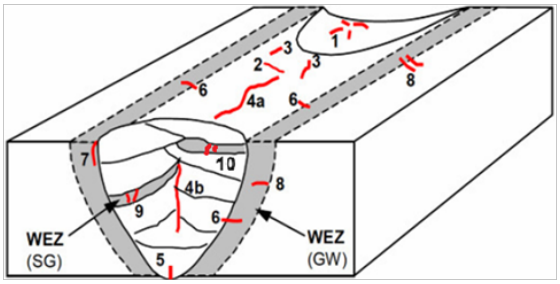

1	Crater crack	Type 1A
2	Transverse crack	Type 1A
3	Longitudinal crack	Type 1A
4a	Longitudinal crack in der middle of weld	Type 1A
4b	Longitudinal crack in der middle of weld (cross section)	Type 1A
5	Crack in the weld root	Type 1A
6	Transverse crack	Type 1B
7	Kantenriss (WAR)	Type 1B
8	DDC in HAZ	Type 2A
9	DDC in HAZ of multilayer weld metal	Type 2C
10	DDC in HAZ of one layer weld metal	Type 2B

Figure 5-1: Hot cracks in welded joints [43]

The fact that the solidification of Alloy 800H is primarily austenitic, causes the susceptibility to hot cracks in similar weld. In particular, the hot cracking is favoured by the high susceptibility of Alloy 800H to form low-melting eutectics, brittle phases and micro-segregations [49].

As already mentioned nickel has a high affinity to sulphur. In this regard, Fink [52] describes how the diffusion of sulphur into the alloy occurs during heat treatment due to sulphur-containing combustion gases or by non-removal of sulphur containing drill emulsions and cutting oils from previous processing steps. The diffusion of sulphur into the alloy occurs along the grain boundaries by formation and deposition of nickel sulphide (NiS). Due to this damage of the grain boundaries, nickel tends to hot cracking during welding or hot forming and tearing during a cold forming process. At the same time, these contaminated grain boundaries are the starting points for corrosion damage [6].

Furthermore, Heubner [53] reports that the diffusion of sulphur starts at a temperature of 550 °C and the eutectic composition of nickel sulphide (Ni_3S_2) melts already at 645 °C.

Zinke [54] examined the influence of nitrogen on the improvement of hot crack susceptibility based on systematic analysis of Alloy 800 welds. The investigations were carried out using the GMAW pulsed arc and TIG welding processes of similar welded samples. The welds of Alloy 800 were made with the comparatively higher alloyed filler SG X15NiCrNb32-21 (mat. no. 1. 4850). The addition of nitrogen was carried out as a component of the mixed inert gas.

The results obtained in [55], [54] show a positive effect of nitrogen on hot crack susceptibility. A significant increase in the hot crack resistance was carried out by mixing only nitrogen for Alloy 601 (NiCr23Fe, mat. No. 24851) and Alloy 602 (NiCr25FeAlY, mat. No. 2. 4633).

On the basis of the investigation from [54] and the programmed-deformation-cracking tests (PDC-test), critical strain rates v_{kr} are demonstrated for, see **Table 5-1**.

Welding process	Shielding gas			Critical strain rate v_{kr} [mm / min]
	Ar	N_2	H_2	
TIG	100	–	–	24
	99	1	–	25
	98	3	–	25
	96,3	3	0,7	23
	95	5	–	21
GMAW	100	–	–	25
	96,3	3	0,7	22
	95	5	–	17
	88	12	–	23
	80	20	–	25

Table 5-1: Critical strain rates for PDC-Test of Alloy 800 [54]

The critical strain rate determined on the basis of the PDC test allows an assertment regarding the resistance to hot cracks of materials, which is calculated from the equation [56], [57]:

$$v_{kr} = a \cdot \frac{L_r}{v_s} \tag{5.1}$$

with the parameters

- a – Acceleration [mm/s^2]
- L_r – Distance from the start of the seam to the occurrence of initial solidification crack [mm]
- v_s – Welding speed [mm/s]

Based on the determined values, see Table 5-1, it can be clearly seen that the addition of nitrogen does not cause any decisive change. According to [58], [59], there is hot crack safety for a welding speed of > 70 mm / min.

Furthermore, there are in addition to the DVS guidelines alternative theories and approaches to the assessment of hot cracking, which are discussed in detail in [59], [60]. A reliable definition is found in all theories for the temperature range at the time of the hot crack formation.

This is the critical temperature interval of brittleness (BTR[9])), or the temperature range of the nil-ductility (NDR), in connection with the hot crack susceptibility [61]. The BTR is limited by the nil-ductility transition temperature (NDT) and the nil-strength temperature (NST).

NDT characterises the temperature at which during the heating no more necking occurs, whereas the NST indicates the temperature upon further heating, at which a significant melting of the grain boundaries occurs, and consequently no load transfer is possible [51]. In [59] the NDT and NST are shown for Alloy 800H, see **Table 5-2**.

[9] BTR - Brittle-Temperature-Range

	NST [°C]	BTR [°C]	RDR [%]
Alloy 800H	1365	115	29,9

Table 5-2: Nil-strength-temperature (NST), brittle temperature-range (BTR) and ratio of ductility recovery (RDR) for Alloy 800H [59]

In addition, in Table 5-2, the ratio of ductility recovery (RDR) is given, which is needed for an accurate characterisation of the susceptibility to hot cracking and can be calculated by the principle illustrated schematically in **Figure 5-2**.

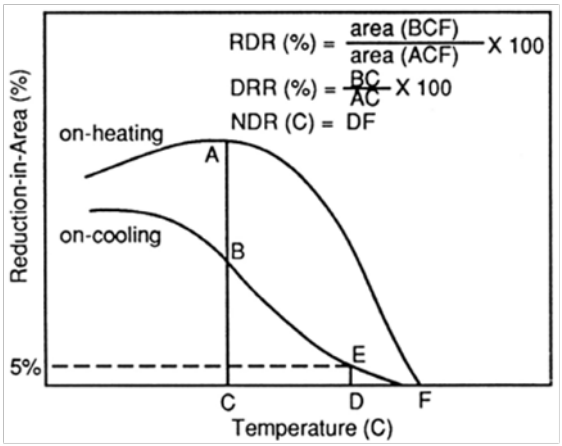

– RDR = ration of ductility recovery,
– DRR = ductility recovery rate,
– NDR = nil ductility range (or BTR),
– Point F = nil ductility temperature (NDT) on-heating,
– Point D = ductility recovery temperature on-cooling

Figure 5-2: Hot forming profiles for determination of hot cracking-susceptibility [59]

The calculated cooling curves for the characteristic values indicated in Table 5-2 are shown in **Figure 5-3**.

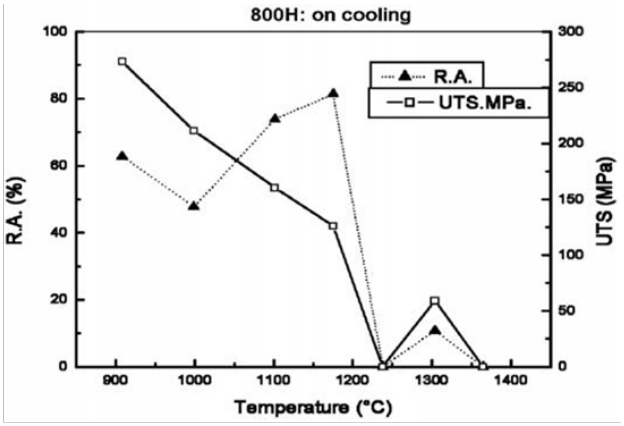

Figure 5-3: High temperature strength and reduction of area of Alloy 800H during the cooling phase [59]

In the investigations carried out, a strong grain growth was observed in the range of NST with formation of thin films and cavities along the grain boundaries, see **Figure 5-4**.

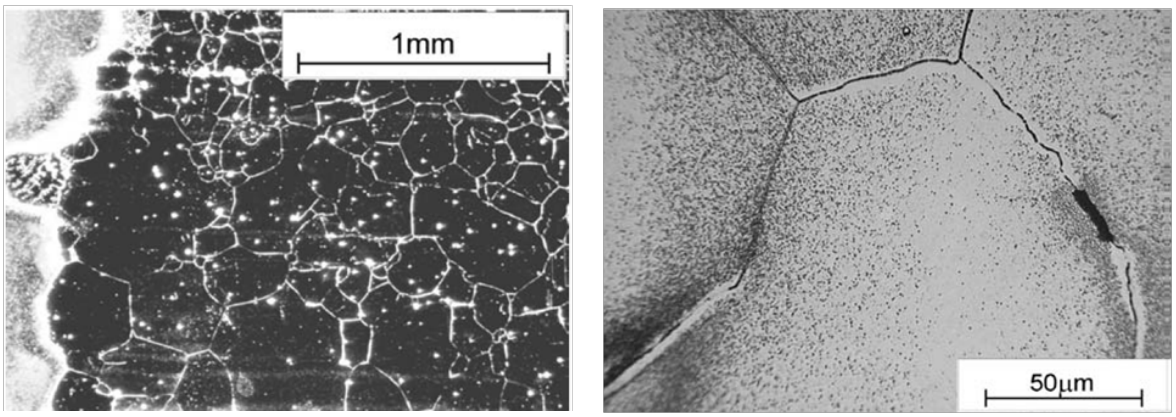

Figure 5-4: (a) Grain growth in the base material Alloy 800H at NST,
(b) Film- and cavity formation along grain boundaries [59]

Since no coalescence was observed, the grain boundaries can be described as the weakest point. Furthermore, at temperatures below NST longitudinal cracks occurred along the precipitation bands, which are intercrystalline and oriented in transverse direction, see **Figure 5-5**.

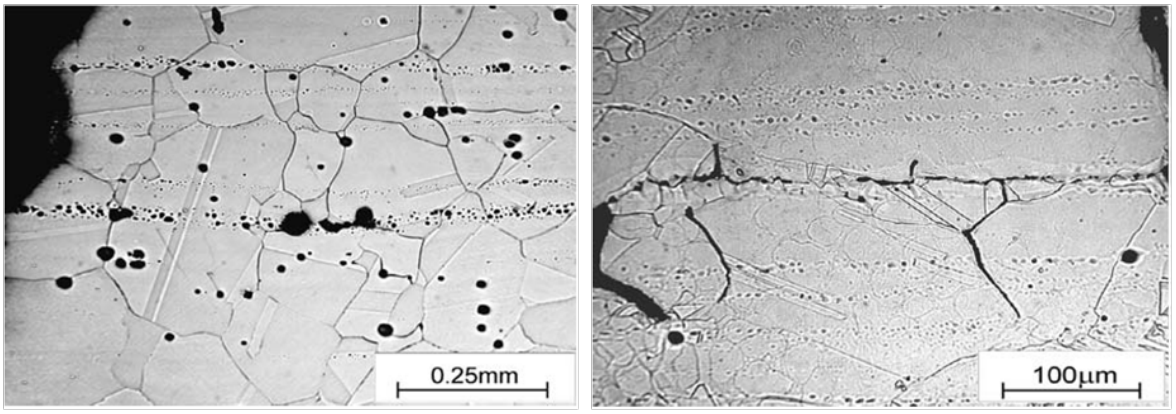

(a) (b)

Figure 5-5: (a) Cavities in precipitation bands near fracture of tensile specimen at NST, (b) longitudinal cracks along precipitation bands and cross intercrystalline cracks, tested at 1200 °C [59]

In nickel base materials there is also a high tendency to formation of liquation cracks in the HAZ. Lundin [37] examined the susceptibility of Alloy 800 H to liquation cracks using the Varestraint test, see **Figure 5-6**.

Lundin [37] showed that a strong dissolving of the precipitates in the HAZ at higher heat input in the weld can be detected, which leads to a loss of cohesion. At the same time an increase in susceptibility to liquation cracks occurs in the HAZ due to the dissolving of precipitates and the associated redistribution of solute elements. In particular, this susceptibility is promoted by redistribution of titanium and niobium rich carbides along the grain boundaries.

Furthermore, there is a correlation between tendency to formation of liquation cracks and the grain size in the melting zone next to HAZ. The liquation crack susceptibility of Alloy 800 H can be minimized by a controlled grain size in the HAZ. Here, a smaller grain size improves the melting crack resistance of the base material in the HAZ [37].

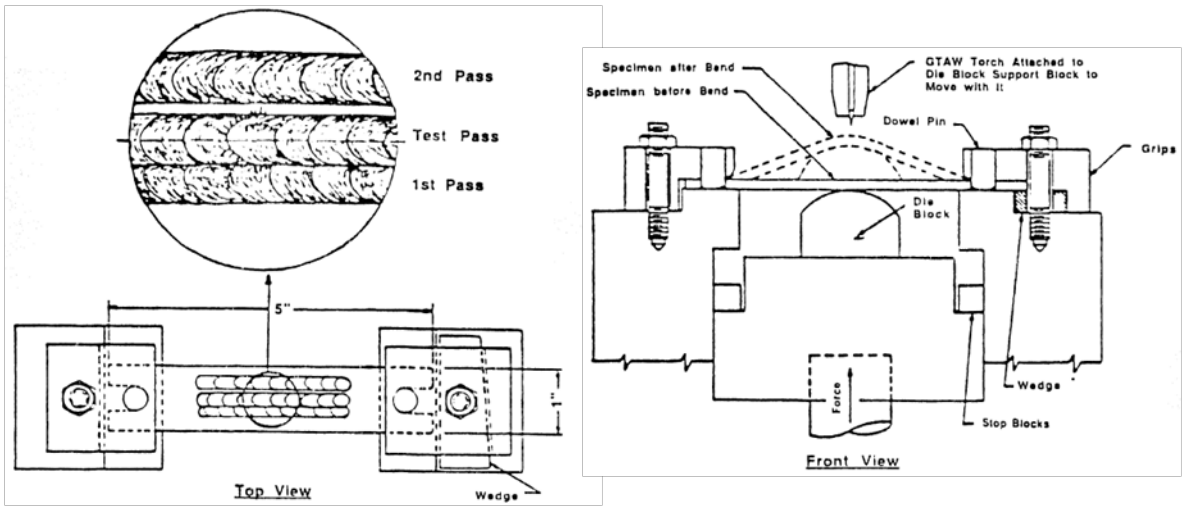

Figure 5-6: Schematic diagram of the Varestraint test apparatus and -method [37]

Lundin [37] has compiled a comprehensive summary of the trace and alloying elements of Alloy 800H affecting the hot cracking tendency and shown their influences. In summary, the most important elements for the Ni-Fe-Cr alloys are: S, P, B, Nb, Ti, N, C, Si, O and Mo. **Table 5-3** lists all trace and alloying elements according to the their influence.

Beneficial	Insignificant	Controllable	Detrimental
Nb	Mn	Al	Pb
Mg	Cu	Ti	S
Cr	C	P	
Fe	Mo	Zr	
Co	Si	B	

Table 5-3: Hot crack influencing elements of nickell alloys [37]

Kujanpää et al. [61] show the solidification cracking propensity of the HAZ as a function of the total content of the impurities sulphur (S) and phosphorus (P) and the Cr_{eq} / Ni_{eq} ratio, see **Figure 5-7**. The solid line represents the boundary between the primary austenitic and ferritic solidification.

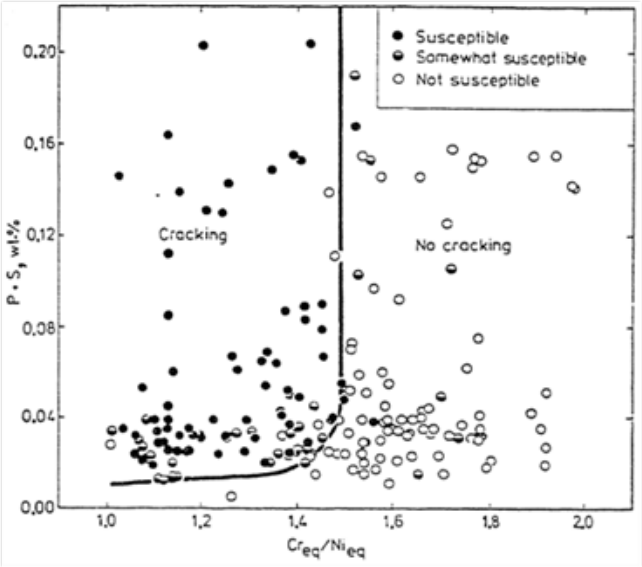

Figure 5-7: Correlation between solidification mode, the P+S-content and crack susceptibility [37]

The susceptible alloys for solidification cracking have a $Cr_{äq}$ / $Ni_{äq}$ ratio of less than about 1.50. If the total content of P + S is kept below 0.01% in these alloys, it is not expected that even in fully austenitic alloys solidification cracks occur in the HAZ [37].

In accordance with the results of Kujanpää the welding tests carried out by Lundin show sulphur and phosphorus segregations along the grain boundaries in areas with hot cracks. Thus, sulphur and phosphorus are essential for solidification cracking in the HAZ.

In [62] the susceptibility of different alloys, including Alloy 800H, to solidification cracking has been examined. In this programme, different procedures were used and a ranking of the susceptibility of the tested alloys was set up. The procedures used here were: Varestraint test, Transvarestraint test, modified Varestraint-Transvarestraint-test, cast pin tear test (CPTT), programmed deformation cracking test (PDC), as well as the hot cracking test methods of the State technical Bauman Moscow University (MIS 1 and LTP-1-6).

To summarise the results, Alloy 800H can be considered as the alloy with the highest susceptibility, followed in descending order by alloys 926, AC66 and 825. **Figure 5-8** shows the ratio of the alloys tested by CPTT method.

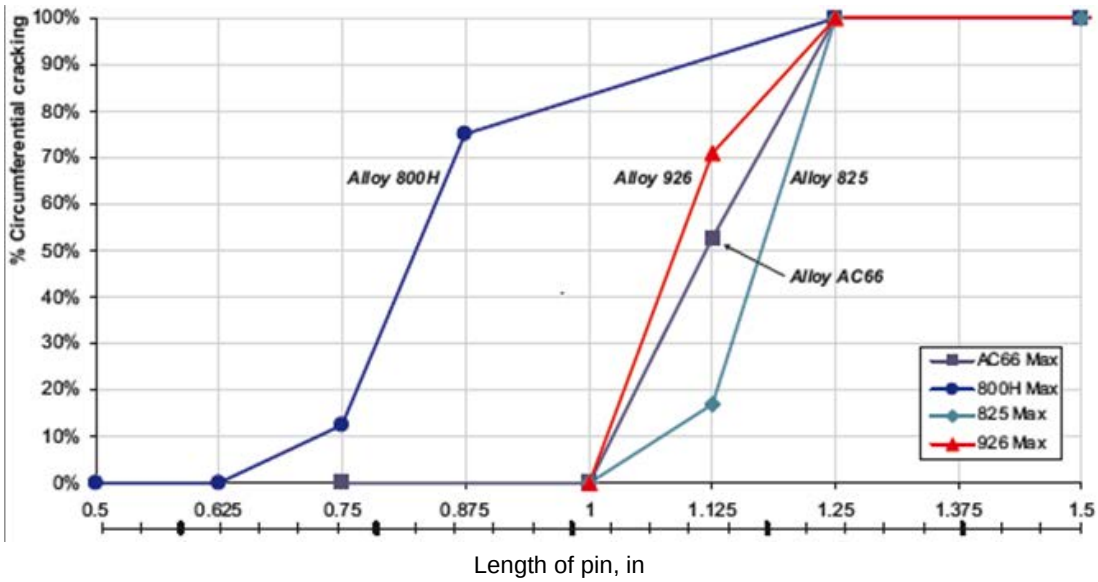

Figure 5-8: Solidification crack- susceptibility by CPTT [62]

According to [3] hot cracks of type 2 are known internationally as Ductility Dip Cracks (DDC). In [50] the formation of DDC occurs far below the effective solidus temperature, caused by a drop of plasticity within a critical temperature range (DTR[10]), see **Figure 5-9**. Meanwhile, the formation of hot cracks of the type I occurs at a temperature above half the specific melting temperature of the base metal in a temperature range of brittleness (BTR).

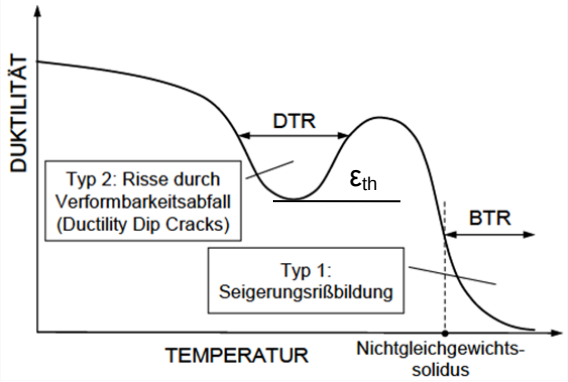

Figure 5-9: Schematic hot plasticity curves of DDC and marked strain threshold ε_{th} [62]

Collins, Lamont, and Ramirez [63], [64], [65] published a three-part article on nickel base filler materials and their susceptibility to ductile dip cracking (DDC). They investigated two filler materials, filler INCONEL 82(2. 4806) as standard designed for welding Alloy 800H and filler INCONEL 52. The samples were tested on the basis of the strain to fracture (STF), a process developed in 2002 at Ohio State University to assess the susceptibility of filler materials compared to DDC [66].

In the first part, Collins [63] showed that the orientation of the grain boundaries to the direction of loading is a decisive factor for the formation of DDC. The grain boundaries most susceptible to DDC during the subsequent investigations had an orientation of 45-90 ° to the applied strain direction [65]. The triple points of the grain boundaries also represent areas with a high concentration of stress, which promote the formation of cracks [65]. Furthermore, the results show that the susceptibility to DDC is significantly increased by the addition of hydrogen and sulphur. Intercrystalline cracks are formed at the triple points of grain boundaries and deep cavities occur [63].

In the second part Collins [64] investigated the influence of temperature on the damage behaviour of the DDC. It could be demonstrated in the studies that the DDC damage may be classified in three temperature ranges, low (625-800 °C), medium (850-1000 °C) and high (1050-1200 °C). The fracture appearance at low and high temperatures is ductile intercrystalline with ductile pits and sharp-edged forms. However, in the intermediate temperature range, fracture shows ductile intercrystalline cavities with rounding [65].

In the third part, Collins [65] identified that eutectic constituents in particular the carbides ((Nb,Ti) C) resulting from the filler 2.4806 reduce the susceptibility of the DDC. Thus an increase of the Nb content of more than 1 wt. % and the enhanced formation of niobium rich carbides has a significant effect on the DDC stability. Due to their formation an effective pinning effect of migrated grain boundaries exists. The higher resistance to DDC is due to the pinning effect, the blocking of weld metal grain boundaries, whereby grain boundaries movement and a grain boundary sliding are prevented at elevated temperatures. Because of the pinning effect on boundaries by niobium-rich M (C, N) carbides, reinforced convoluted boundaries are formed at the end of solidification.

This influence of the precipitates and the different grain boundaries on the resistance to DDC are shown in **Figure 5-10**.

[10] DTR - Ductility Temperature Range

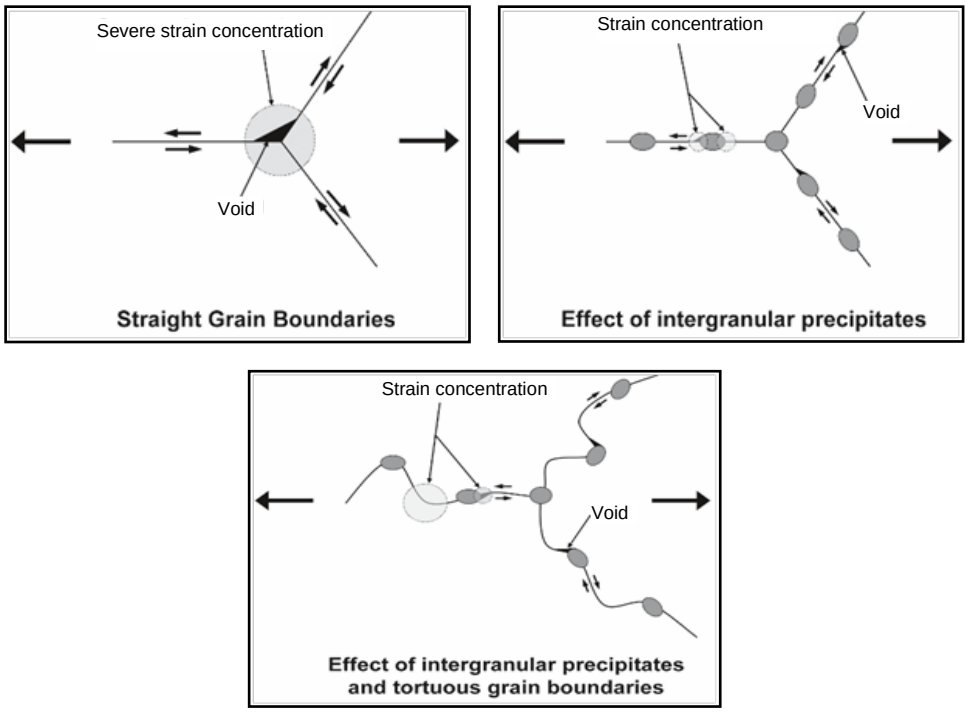

Figure 5-10: Schematic diagram of the influence of grain boundaries and precipitations and on the DDC formation [65]

It is assumed that an increased precipitation of $M_{23}C_6$ carbides on the grain boundaries, resulting from the addition of Mo and B, increases grain boundary binding.

Nissley et al. [67], [68], [69] determined that the threshold strain ε_{th} and the DTR, see Figure 5-9, are two primary quantitative characteristics for how susceptible an alloy is to DDC. Secondary phases do not have any effect on DDC.

The results of the STF tests of various filler materials and the Ductility Dip Cracks occurring are shown in **Figure 5-11**.

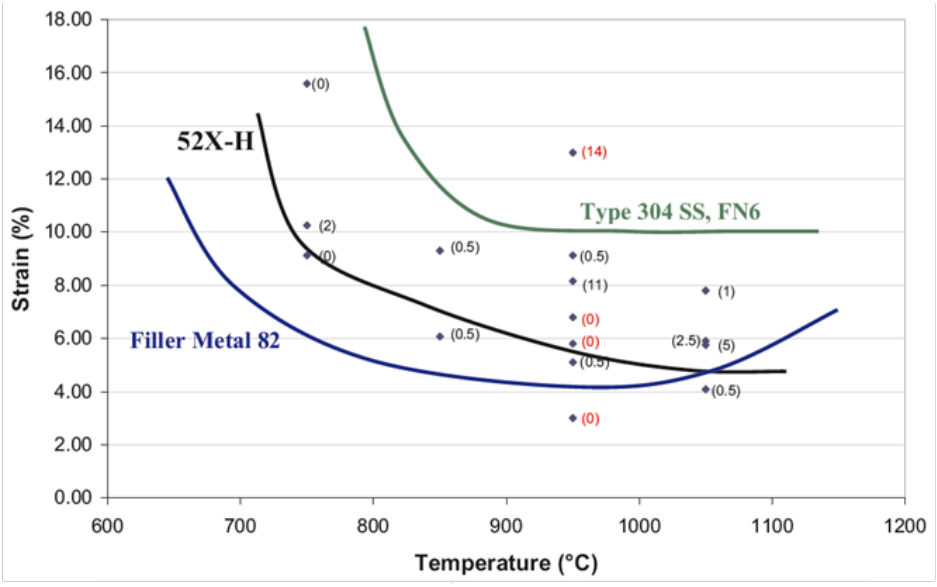

Figure 5-11: Comparison of STF results of filler materials 52X-H, 304L and 82 [70]

The numbers in brackets stand for the number of ductility dip cracks present.

5.2. Relaxation cracks

Relaxation cracks are cold cracks in the coarse grain of the HAZ, caused by precipitation hardening. The high heat input during welding requires first a dissolving of carbides in the area near the fusion line, which do not precipitate completely by too rapid cooling. During a stress-relief heat treatment re-precipitation processes occur. These precipitates cause a strong strain hardening of the grain, allowing relaxations to take place via grain boundary sliding. Due to the relatively low strength and lower deformation resistance of grain boundaries, crack formation occurs in these areas if grain boundary strength is exceeded by residual stresses [71], [72].

In [73] a study of relaxation cracks on a tube of Alloy 800 is described. Because of the low operating temperature of 520°C and an operating period of 18 months the formation of γ 'phase occurred in combination with a loss of ductility in the material. Fracture surface of the relaxation crack is described as granular with grain boundaries which are covered with 7-8 µm wide flat dimples initiated due to fine precipitations. Because of this dimples, there was a small amount of deformation and a significant increase in hardness, which macroscopically was seen as brittle fracture.

The cause of this damage was a selective precipitation hardening with a hardened grain interior and a soft grain boundary section and local excessive stresses for the production of creep strains on the grain boundaries. In addition to the metallurgical conditions grooves caused by mounting caused stress concentrations.

The occurrence of stress relaxation cracks in a temperature range from 500 to 700 ° C is also described in [23].

This type of crack formation is distinguished by manufacturing-related or operational crack formation. Cracks that occur during manufacture, are referred to as reheat, strain relief or relaxation cracks. However, operational cracks are referred to stress relaxation cracks, creep embrittlement cracks, stress-induced cracks, or stress-assisted grain boundary oxidation crack formation [23], [76].

This crack formation is the result of stress reduction caused by a heat treatment after welding, or due to appropriate operating temperatures, particularly in thick-walled components.

Mainly, relaxation cracks occur in coarse-grained areas of HAZ in which intracrystalline precipitates increase the hardness and hence creep deformation occurs exclusively along grain boundaries. A large grain size also minimizes ductility which leads to an increased susceptibility to relaxation cracks [23].

According to descriptions [23] there are four options to reduce the susceptibility to cracking in Alloy 800H:

- Total content of Al + TI less than 0.7%
- Perform stabilization annealing
- Use appropriate filler
- Heat-treatment after welding.

.
Usually the total content of Al + TI is controlled to ≤ 0. 7 wt % in Alloy 800H, but attention should be given to the susceptibility of relaxation cracks. In terms of stabilisation annealing of the base material, a heat treatment at 980 °C for 3 hours after forming operations is recommended [23]. Hereby a precipitation of coarse carbides at the grain boundaries is intended, whereby the fine precipitates are reduced in the grain interior at later operating temperatures. After forming above 15 % instead of stabilising annealing a solution annealing at a temperature of 1150 to 1200 °C should be carried out.

According to [23] considering filler materials, higher alloyed filler metals ENiCrFe-3 (e.g. INCONEL 182) from the standard recommendation are suitable for operation above 760 °C, however promote the susceptibility to cracking at temperatures 538-704 °C.

For operation of Alloy 800 H in a temperature range from 538 to 704 °C therefore a filler metal is recommended which exactly corresponds to the chemical composition of the base material, in particular the chromium and nickel values.

Heat treatment after welding is recommended as the most effective prevention against operational relaxation cracks, however, it entails the risk of relaxation cracks during production. As a minimum, up to a material thickness of 25 mm, a temperature of 885 °C for a duration of 1 – 1,5 hours is recommended. For material thicknesses greater than 25 mm, an increase in the duration of +0.04 h / mm is recommended. The cooling and heating rates to be applied should be agreed with the semi-finished product manufacturers.

In [23] it is reported that Alloy 800 shows sufficient ductility and no crack formation at operating temperatures above 788 °C.

Summary

- *Exceeding the critical deformation speed v_{kr} of ca. 25 mm/min for the TIG welding process and ca. 23 mm/min for the GMAW-welding process increases the risk of hot cracks formation in Alloy 800. .*
- *Alloy 800H has a critical temperature interval of brittleness of 115 ° C and a nil-strength temperature of 1365 ° C, at which thin films and cavities form along the grain boundaries.*
- *The high sensitivity of Alloy 800 H to form low-melting eutectics, brittle phases, as well as micro segregations promotes the segregation induced cracks (hot crack type I).*
- *The resistance to melting cracks is increased by a smaller grain size in the HAZ of the base material.*
- *Solidification cracks are not expected if a total content of P + S is maintained below 0.01%.*
- *Hot cracks of type II (Ductility Dip Cracks) occur mainly on the triple points of grain boundaries with an orientation of 45-90 ° to the applied strain direction.*
- *Carbides at the grain boundaries increase the resistance/ stability to DDC due to a pinning effect, which blocks the grain boundary sliding.*
- *By using the filler material 2.4806 and by not exceeding a strain of 4% no ductility dip cracks are expected.*
- *The occurrence of relaxation cracks is expected in the coarse grain zone at a temperature range between 500 to 700 ° C. Most effective prevention is a heat treatment at about 885°C for residual stress reduction.*
- *For operating temperatures above 788°C relaxation cracks are not expected in Alloy 800.*

6. Heat treatment

According to DVS regulations 931 [36], due to the risk of the formation of undesirable precipitates (e.g. intermetallic phases) no heat treatment is recommended for fully austenitic materials. In contrast in exceptional cases an annealing treatment can be carried out to reduce high stresses. This should be in agreement with the manufacturers of materials and filler metals. Thermal levelling of stainless steels with an acetylene-oxygen flame is unproblematic. It is only necessary to ensure that the surface is cleaned before levelling and the levelling is carried out with a neutral or slightly excess oxygen flame to avoid carburization [36].

6.1. Heat treatment before welding

Characteristic for the nickel alloys is work hardening during various cold forming processes. The strain hardening increases with the complexity of the alloy and with increasing carbon content. Due to this the nickel alloys require an intermediate annealing to induce a recrystallization and to soften the material for further cold working [3].

If non-age-hardenable austenitic high-temperature materials are not suitable for soft or recrystallization annealing, these are delivered in the solution annealed condition, whereby the desired grain size is achieved and the carbon is dissolved [53]. The solution annealing temperature of Alloy 800 H is 1150°C with a holding time of approx. 30 to 60 min [2], [53], [75].

The literature [3] as well as the manufacturer [2] recommended quenching in water after solution annealing. In particular the temperature range between 760 up to 540 °C should be passed through quickly. This prevents the formation of $M_{23}C_6$ carbides during cooling and achieves a resistance to intercrystalline corrosion. In addition for material thicknesses under approximately 1.5 mm the cooling can be carried out in air [2].

In [16] the reduction of the solution annealing temperature at complete recrystallization is described as a positive influence on the resistance of Alloy 800H to intercrystalline stress corrosion cracking. Thus, smaller grain sizes occur due to low annealing temperature which is a positive effect. The lower the solution annealing temperature the more titanium binds the carbon. This reduces the precipitation of grain boundary carbides.

6.2. Heat treatment after welding

By use of austenitic high-temperature materials at low temperatures (550 to 780 °C), it is assumed that Alloy 800 H tends to crack formation due to relaxation and precipitation processes [53], [76]. In particular stress relaxation cracks can be expected if cold-forming and / or welding of the material were carried out [55]. A preventive procedure can be an intermediate stabilising annealing.

For stabilizing of Alloy 800H an annealing is recommended at 980 °C for 3 hours, according to [53].

If the intention is to use Alloy 800H at temperatures below 600 °C, or in the area of wet corrosion, a soft annealing at a temperature of 960 °C is recommended as a final treatment for stabilisation of the material. By precipitation of carbides a possible susceptibility of the material should be prevented. The more the material tends to precipitations the higher the cooling rate must be chosen [53].

In the context of intercrystalline stress corrosion cracking [3], a heat treatment in the temperature range of carbide precipitation, 600 to 800 °C can be performed. The $M_{23}C_6$ carbides are located in discrete, spherical form at the grain boundaries and prevent crack susceptibility.

For Alloy 800H it is described [3] that when operating temperatures above 540 °C are planned, the alloy should be heat-treated at a temperature of at least 885°C after welding. The $M_{23}C_6$ carbides precipitated appear as block-shaped, discrete particles instead of films leading to the formation of stress relaxation cracks.

For use of Alloy 800 H in power plant technology a stress relief heat treatment is recommended [53], if, e.g. tubes slightly drawn or in exceptional cases in hard state were used, or if inadmissible residual stresses

occurred. Residual stresses can be reduced by a stress relief heat treatment at temperatures of 540 °C, but a complete removal of residual stresses can be guaranteed only with the help of a soft annealing and the associated recrystallization. In this course, a susceptibility of the material must be avoided at the same time.

Schubert [34] investigated possible cracks in the HAZ of Alloy 800. He recommends a stress relief heat treatment in the temperature range between 750 and 850 °C for weld seams larger than 10 mm at operation temperatures below 700 °C. The reason is the insufficient relaxation of the residual welding stresses below this temperature.

Furthermore, it is recommended that in addition to stress relief heat treatments the components are designed over the entire temperature range so that shrinkage of 0.04% is possible.

Summary

- *In principle no heat treatment is recommended for fully austenitic materials. In exceptional cases, a heat treatment can be performed to reduce residual stresses.*
- *For a complete recrystallization of Alloy 800H (base material) a solution heat treatment is to be carried out at a temperature of 1150 °C and a holding time of about 30 - 60 min followed by quenching in water.*
- *To prevent relaxation cracks at temperatures between 500 and 700 °C a stabilized annealing for 3 hours at 980 °C can be performed. The objective is a precipitation of coarse carbides at the grain boundaries and a reduction of subsequent precipitation of fine carbides in the grain interior.*
- *To reduce residual stresses a stress relief heat treatment can be carried out at temperatures between 750 and 850 ° C.*

7. Conclusion

Based on a literature review, the causes and the effects of the microstructure on the crack initiation in welds of the nickel based Alloy 800H should be explored and avoidance measures proposed.

On the basis of the available literature a compilation of metallurgical and welding measures to improve crack susceptibility and to avoid the formation of cracks during and after welding could be created. As conclusions the following scientific/ technical results are listed below:

1. Alloy 800 H is a solid solution strengthening Ni-Fe-Cr alloy with a face centred cubic lattice structure, with a grain size between 70 to 180 µm and twin grains present in the microstructure. The austenitic matrix includes mainly titanium carbonitrides (TI (C, N)), chromium-rich mixed carbides ($M_{23}C_6$) and γ'-phase (Ni_3 (TI, Al)). Other intermetallic phases, such as G-phase and σ-phase have been reported to exist after long-term exposure. The precipitation processes could be described by the TTT-diagrams. The precipitation of the $M_{23}C_6$ carbide occurs in particular on and along the grain boundaries in the temperature range 550 - 1100 °C. Carbides TiC precipitates only from temperatures above 700 °C and mostly within the grain. A precipitation of γ'-phase can be expected only in a temperature range of 440 to 650 °C.

2. The welding processes for the production of similar and dissimilar weld joints of Alloy 800H used in the literature were determined and presented. In addition to special welding processes, conventional welding processes MIG, TIG and MMA were used. The recommended welding parameters used in the literature and the filler materials, their microstructure and the influence on crack formation were discussed. The filler metal 2.4806 was mainly used by recommendation in standards and from manufacturers of semi-finished products. The weld strength factor for the welded joint for Alloy 800H could be shown for a creep rupture strength of 100,000 h within temperature range from 600 to 1000 °C for different welds.

3. For the assessment of crack susceptibility of Alloy 800H a critical strain rate v_{kr} could be demonstrated as a criterion for the formation of hot cracks. The critical temperature interval of brittleness and the nil-strength temperature could be determined and the behaviour of the material, the formation of thin films and cavities along the grain boundaries could be described. Regarding the hot cracks type I the influence of accompanying elements and the need for compliance with the total content of P+S < 0.01 % to prevent solidification cracks were presented. The cause of the cracks of hot type II (DDC) was shown, the context with the grain boundary types present explained and the influence of impurities and the pinning effect of carbides demonstrated. Thus the occurrence of DCC is not expected in a temperature range above 600 °C by use of filler material 2.4806 and a maximum strain of 4 %. No damage due to relaxation cracks is expected at temperatures above 788° C.

4. Of the possible factors influencing the formation of cracks, which can be divided into metallurgical-related and process-related mechanisms, an intermediate stabilising annealing for 3 hours at 980 °C is required to avoid relaxation cracks due to intense welding. To reduce residual stresses a stress relief heat treatment can be carried out, however a full removal can only be achieved by means of soft annealing at 750 to 960 °C, at which attention must be paid to high cooling rates due to a susceptibility of the alloy.

As a result of this detailed literature review, a comprehensive overview of published articles, research reports and manufacturer's specifications and recommendations, standards and guidelines for the nickel base alloy Alloy 800 H is given. It also provides a comprehensive overview of the possibilities for welded structures made of Alloy 800 H.

8. References

[1] Stahl-Eisen-Werkstoffblatt 310: Werkstoffe mit besonderen physikalischen Eigenschaften, Verlag Stahleisen GmbH, Düsseldorf

[2] Werkstoffblatt Nr. 4129: Nicrofer® 3220 H, Korrosionsbeständige Legierungen ThyssenKrupp VDM GmbH, Werdohl, pp. 2-11, 2003

[3] DuPont, J. N., J. C. Lippold and S. D. Kiser: Welding Metallurgy and Weldability of Nickel-Base Alloys, John Wiley & Sons, Inc., pp. 26-75, 2009

[4] http://www.springermaterials.com/docs/VSP/datasheet/lpf-c/01100000/LPFC_1100735.html

[5] Data Sheet Number SMC-047: INCOLOY® alloy 800H & 800HT®Special Metals Corporation, pp. 1-12, 2004

[6] Bargel, H.J. and G. Schulze: Werkstoffkunde, Springer + Vieweg Verlag, Heidelberg, 11. Auflage, pp. 104-323, 2012

[7] Roy, A.K. and V. Virupaksha: Performance of alloy 800H for high-temperature heat exchanger applications, Materials Science and Engineering, Elsevier, pp.1-8, 2007

[8] Gan, J. et al.: Irradiated microstructure of alloy 800HJournal of Nuclear Materials, Elsevier, pp.1, 2006

[9] Tan, L. et al.: Microstructure tailoring for property improvements by grain boundary engineering Journal of Nuclear Materials, Elsevier, pp.1, 2008

[10] Drabble, D. J., C. M. Bishop and M. V. Kral: A Microstructural Study of Grain Boundary Engineered Alloy 800HThe Minerals, Metals & Materials Society and ASM International, Vol. 42A, pp. 763-772, 2011

[11] Büringer, E., X. Wang and G. Gottstein: Nucleation mechanisms of dynamic recrystallization in austenitic steel alloy 800H, Acta Metallurgica Inc., Pergamon, Scripta Materialia,Vol. 38, pp.2-3, 1998

[12] Wang, X., E. Brünger and G. Gottstein: Microstructure characterization and dynamic recrystallization in an Alloy 800H, Materials Science and Engineering, Elsevier, pp.1-6, 2000

[13] Wang, X., E. Brünger and G. Gottstein: The role of twinning during dynamic recrystallization in alloy 800H, Acta Metallurgica Inc., Pergamon, Scripta Materialia, Vol. 46, pp. 5, 2002

[14] Tan, L. et al.: Microstructure optimization of austenitic Alloy 800H (Fe-21Cr-32Ni), Materials Science and Engineering A 528, Elsevier, pp.1, 2011

[15] Koehler, W.: Analyse des Einflusses der Schneidform auf den Hochleistungsbohrprozess Vulkan Verlag Essen, pp. 8, 2005

[16] Carlén, J. C. and U. Blom: Einfluss von Analyse, Wärmebehandlung und Gefüge auf die Empfindlichkeit für interkristalline Spannungsrißkorrosion von Nickel-Chrom-Eisenlegierungen (Alloy 800 und Alloy 600), Zeitschrift für Werkstofftechnik, Verlag Chemie GmbH, Weinheim, pp. 412, 1973

[17] Aigner, H., O. Demel and H. P. Degischer: Einfluss einer Auslagerung unter Schutzgas bei 800 bis 1000 °C auf die mechanischen Eigenschaften des Werkstofftyps X 10 NiCrAlTi 32-20, Zeitschrift für Werkstofftechnik, Verlag Chemie GmbH, Weinheim, pp. 1-8, 1983

[18] Taylor, N. G. et al.: The Creep Ductility and Fracture of Carburised Alloy 800H at High Temperatures, High Temperature Alloys, Elsevier, pp. 475-486, 1985

[19] Teneva-Kosseva, G. I.: Oxidschichtbildung und Materialprobleme, metallischer Werkstoffe bei Verbrennungsprozessen mit Heizöl, EL Dissertation, HS-Aachen, pp. 23-24, 2005

[20] Dehmolai, R., M. Shamaniana and A. Kermanpura: Microstructural changes and mechanical properties of Incoloy 800 after 15 years service, Materials Characterization 60, Elsevier, pp. 1-5, 2009

[21] Werkstoffblatt Nr. 4110: Nicorros®-alloy 400, Korrosionsbeständige, Legierungen ThyssenKrupp VDM GmbH, Werdohl, pp. 4, 2003

[22] Baker, B.: Personal email communication Special Metals Corporation, Huntington, 2010.

[23] API PUBLICATION: Materials, Fabrication, and Repair Considerations for Hydrogen Reformer Furnace Outlet Pigtails and Manifolds API-Komitees-Draft, pp. 10-12, 2011

[24] Timmins, P. F.: Solutions to Equipment Failures, ASM International, pp. 112, 1999

[25] Islam, M.: Thermal Fatigue Failure of Alloy UNS NO8800 Steam, Superheating Tubes CC Technologies, Handbook of Case Histories in Failure Analysis, Vol. 2, ASM International, pp. 238, 1992

[26] Lippold, J.C.: Materials Performance NACE International, Vol. 24 (No. 10), pp. 16, 1985

[27] Orr, J.: A Review of the structural characteristics of Alloy 800 Alloy 800, North-Holland Publishing Company, Elsevier, pp. 72, 1978

[28] Jones, W.B. und R. M. ALLEN: Mechanical Behavior of Alloy 800 at 838 K Metallurgical Transactions A, Vol. 13A, pp. 10, 1982

[29] Nicolin, G. et al.: Entwicklung der Mikrostruktur in Alloy 800HT unter Hochtemperaturkriechbeanspruchung, WILEY-VCH Verlag GmbH, Weinheim, pp. 4-7, 1998

[30] API PUBLICATION: Materials, Fabrication, and Repair Considerations for Austenitic Alloys Subject to Embrittlement and Cracking in High Temperature 565 - 760°C API-Komitees-Entwurf, pp. 20, 2012

[31] Mizia, R. E. et al.: Optimizing the Diffusion Welding Process for Alloy 800H, Metallurgical Transactions A, Vol. 44A, pp. 154-159, 2011

[32] Van Wortel, H.: Control of Relaxation Cracking in austenitic high temperature components, pp. 10, 2007

[33] Christ, H. J.: Werkstoffeinsatz bei hohen Temperaturen Vorlesungsskript Universität Siegen, pp. 50, 2013

[34] Schubert, J.: Prüfbericht Alstom Power System GmbH, pp. 1-17, 2011

[35] SFI-Aktuell 2008 Verband für Schweißen und Verwandte Verfahren e.V., DVS Verlag, pp. 113-470, 2008

[36] DVS-Merkblatt 931 Verband für Schweißen und Verwandte Verfahren e.V., pp. 2-7

[37] Lundin, C. D. and C. Y. P. Qiao: Evaluation of HAZ Liquation Cracking susceptibility and HAZ Softening behavior in modified 800H, Report University of Tennessee, pp. 38-106, 1993

[38] Sireesha, M. et al.: A comparative evaluation of welding consumables for dissimilar welds between 316LN austenitic stainless steel and Alloy 800, Journal of Nuclear Materials, Elsevier, Vol. 279, pp. 2-11, 1999

[39] Sireesha, M. et al.: Microstructural features of dissimilar welds between 316LN austenitic stainless steel and alloy 800, Journal of Nuclear Materials, Elsevier, Vol. 292, pp. 1-8, 2000

[40] Sireesha, M., S. K. Albert and S. Sundaresan: Influence of High-Temperature Exposure on the Microstructure and Mechanical Properties of Dissimilar Metal Welds between Modified 9Cr-1Mo Steel and Alloy 800, Metallurgical Transactions A, Vol. 36A, pp. 1-12, 2005

[41] Schmidt, K.: Komponentenverhalten im 700 °C-Kraftwerk, Dissertation Universität Stuttgart, pp. 87, 2013

[42] Tillack, D. J.: Nickel alloys and stainless steels for elevated temperature service: weldability considerations, Tillack Metallurgical Consulting, Inc., pp. 6-12, 1997

[43] AiF-Report: Werkstoff- und fügetechnische Analyse und Optimierung eines Reformers für Brennstoffzellenanwendung, 16118BG, pp. 22-92, 2011

[44] DVS-Merkblatt 0912 Verband für Schweißen und Verwandte Verfahren e.V., pp. 2

[45] DVS-Merkblatt 941-3 Verband für Schweißen und Verwandte Verfahren e.V., pp. 5

[46] DIN EN ISO 18274:2010: Schweißzusätze DIN Deutsches Institut für Normung e. V., pp. 11-16, 2011

[47] UTP Schweissmaterial: NiCr-Schutzgasdraht für korrosionsbeständige und hochwarmfeste Werkstoffe UTP A 068 HH, Böhler Schweisstechnik Deutschland GmbH, pp. 1, 2010

[48] UTP Schweissmaterial: Vollaustenitischer Schutzgasdraht für Hochtemperaturwerkstoffe UTP A 2133 Mn, Böhler Schweisstechnik Deutschland GmbH, pp. 1, 2010

[49] http://www.erl-gmbh.de/home/fachwissen/berechnungen/streckenenergie/erklaerungen.html

[50] Gruss, H.: Schweissgerechte Struktur- und Prozessstrategien im Flugzeugbau, Dissertation Universität Magdeburg, pp. 24-25, 2008

[51] DVS-Merkblatt 1004-1 Verband für Schweißen und Verwandte Verfahren e.V., pp. 2

[52] Fink, C. and M. Zinke: Wärmereduziertes MAG-Schweißen der heißrissempfindlichen Ni-Basislegierung Alloy 625 (2.4856), Report Universität Magdeburg, pp. 1, 2011

[53] Heubner, U., J. Klöwer: Nickelwerkstoffe und hochlegierte Sonderedelstähle, Expert-Verlag, 4. Auflage, pp. 31, 2009

[54] Zinke, M. et al.: Erhöhung der Heirissbeständigkeit von hochwarmfesten Ni-Basislegierungen durch die Anwendung stickstoffhaltiger Schutzgase beim Schweißen, Schweißen und Schneiden 2003, DVS-Bericht 225, S. 249-250, 2003

[55] Wolf, M.: Zur Phänomenologie der Heißrissbildung beim Schweißen und Entwicklung aussagekräftiger Prüfverfahren, BAM-Dissertationsreihe, Band 19, Berlin, pp. 16-72, 2006

[56] Pshennikov, A.: Entwicklung von Maßnahmen zur Heißrissvermeidung beim Einseitenschweißen langer Schweißnähte, Dissertation Universität Magdeburg, pp. 40, 2005

[57] Schulze, G.: Die Metallurgie des Schweißens, Springer Verlag, 3. Auflage. pp. 568, 2004

[58] Hübner, A.: Untersuchungen über den Einfluss und die Wirkungen von Stickstoffzusätzen im Schutzgas auf das Heißrissverhalten ausgewählter heißrissempfindlicher Nickel-Basiswerkstoffe, Dissertation Universität Magdeburg, pp. 32, 2005

[59] Böllinghaus, T. and H. Herold: Hot Cracking Phenomena in Welds, Springer-Verlag, pp. 55-364, 2005

[60] Hilbinger, R. M.: Heissrissbildung beim Schweissen von Aluminium in Blechrandlage, Herbert Utz Verlag, pp. 31, 2001

[61] Kujanpää, V. P., S. A. David and C. L. White: Formation of Hot Cracks in Austenitic Stainless Steel Welds-Solidification Cracking, Welding Research Supplement, pp. 2-6, 1986

[62] Hilbinger, R. M. et al.: Hot Cracking Phenomena Welds II, Springer-Verlag, pp. 203-413, 2008

[63] Collins, M. G. and J. C. Lippold: An Investigation of Ductility Dip Cracking in Nickel-Based Filler Materials - Part I; The strain-to-fracture test has been used to develop temperature-strain relationships for ductility dip cracking, Welding Research, pp. 1-8, 2003

[64] Collins, M. G., A. J. Ramirez and J. C. Lippold: An Investigation of Ductility Dip Cracking in Nickel-Based Weld Metals — Part II; Fracture behavior and fracture surface morphology are related to microstructure, composition, and temperature, Welding Research, pp. 1-7, 2003

[65] Collins, M. G., A. J. Ramirez and J. C. Lippold: An Investigation of Ductility-Dip Cracking in Nickel-Based Weld Metals — Part III; The characteristics of weld-metal grain boundaries associated with elevated-temperature fracture are investigated, Welding Journal, Welding Research, pp. 1-11, 2004

[66] Fink, C., K. Stein and M. Zinke: Untersuchungen zur Heißrissbildung mit dem Gleeble®3500 Prüfsystem, Otto-von-Guericke-Universität Magdeburg, pp. 7, 2013

[67] Nissley, N. E. and J. C. Lippold: Development of the Strain-to-Fracture Test Welding Journal, Welding Research, pp. 1-10, 2003

[68] Nissley, N. E. and J. C. Lippold: Ductility-Dip Cracking Susceptibility of Nickel-Based Weld Metals Part 1: Strain-to-Fracture Testing Welding Journal, Welding Research, pp. 1-8, 2008

[69] Nissley, N. E. and J. C. Lippold: Ductility-Dip Cracking Susceptibility of Nickel-Based Weld Metals: Part 2 - Microstructural Characterization Welding Journal, Welding Research, pp. 1-10, 2009

[70] Lippold, J.C., and N.E. Nissley: Ductility-Dip Cracking in High Chromium, Ni-Base Filler Metals in Hot Cracking Phenomena in Welds II, pp. 406, 2008

[71] Dilthey, U.: Schweißtechnische Fertigungsverfahren 2: Verhalten der Werkstoffe beim Schweißen, Springer Verlag, pp. 285, 2007

[72] Lange, G.: Systematische Beurteilung technischer Schadensfälle John Wiley & Sons, Inc., pp. 356, 2001

[73] Moeser, M.: Relaxationsrissigkeit an einem Rohr aus hochlegiertem Stahl (Alloy 800) in einer EDC-Spaltanlage, pp. 6, 2009

[74] Krupp, U.: Mikrostrukturelle Aspekte der Rissinitiierung und -ausbreitung in metallischen Werkstoffen, Habilitationsschrift Universität Siegen, pp. 198, 2004

[75] Decking, H. and G. K. Grossmann: Verarbeitungshinweise für austenitische Edelstähle und Nickellegierungen, ThyssenKrupp VDM GmbH, Werdohl, pp. 3-13, 2002

[76] Thier, B.: Apparate: Technik - Bau – Anwendung Vulkan-Verlag Essen, 2. Auflage, pp. 255, 1997

Appendix 1

ISO		Euronorm		
~ X8NiCrAlTi32–21	4955 (1994)	X10NiCrAlTi32–21	10095 –(03/1999)	
United Kingdom		Russia		
X10NiCrAlTi32–21	EN 10095 – (03/1999)			
~ NA 15 H	3074 (1989)			
Japan		China		
~ NCF 800 TP	G 4903 (1991)	~ NS 111	T 15007 (1994)	
~ NCF 800 TB	G 4904 (1991)	~ H01120	T 15007 (1994)	
USA				
ASTM		AMS	SAE	UNS
~ A 240 (N08800)	A 240–02	~ 5766C	~ N08800	~ N08332
~ A 240 (N08810)	A 240–02	~ 5871D	~ N08810	~ N08800

Note: Not in all cases the tolerance range for the chemical composition of steels, used in other countries, corresponds to DIN or EN.

Figure A-1: Comparison of international standards [70]